Stability analysis and inertial regimes in complex flows

by

Iman Lashgari

Dec 2015
Technical Reports
Royal Institute of Technology
Department of Mechanics
SE-100 44 Stockholm, Sweden

Akademisk avhandling som med tillstånd av Kungliga Tekniska Högskolan i Stockholm framlägges till offentlig granskning för avläggande av teknologie doktorsexamen fredagen den 18 December 2015 kl 10.15 i Kollegiesalen, Kungliga Tekniska Högskolan, Brinellvägen 8, Stockholm.

Universitetsservice US–AB, Stockholm 2015

Stability analysis and inertial regimes in complex flows

Iman Lashgari
Linné Flow Centre, KTH Mechanics, Royal Institute of Technology
SE-100 44 Stockholm, Sweden

Abstract

In this work we first study the non-Newtonian effects on the inertial instabilities in shear flows and second the inertial suspensions of finite size rigid particles by means of numerical simulations.

In the first part, both inelastic (Carreau) and elastic models (Oldroyd-B and FENE-P) have been employed to examine the main features of the non-Newtonian fluids in several configurations; flow past a circular cylinder, in a lid-driven cavity and in a channel. In the framework of the linear stability analysis, modal, non-modal, energy and sensitivity analysis are used to determine the instability mechanisms of the non-Newtonian flows. Significant modifications/alterations in the instability of the different flows have been observed under the action of the non-Newtonian effects. In general, shear-thinning/shear-thickening effects destabilize/stabilize the flow around the cylinder and in a lid driven cavity. Viscoelastic effects both stabilize and destabilize the channel flow depending on the ratio between the viscoelastic and flow time scales. The instability mechanism is just slightly modified in the cylinder flow whereas new instability mechanisms arise in the lid-driven cavity flow.

In the second part, we employ Direct Numerical Simulation together with an Immersed Boundary Method to simulate the inertial suspensions of rigid spherical neutrally buoyant particles in a channel. A wide range of the bulk Reynolds numbers, $500 \leq Re \leq 5000$, and particle volume fractions, $0 \leq \Phi \leq 0.3$, is studied while fixing the ratio between the channel height to particle diameter, $2h/d = 10$. Three different inertial regimes are identified by studying the stress budget of two-phase flow. These regimes are laminar, turbulent and inertial shear-thickening where the contribution of the viscous, Reynolds and particle stress to transfer the momentum across the channel is the strongest respectively. In the inertial shear-thickening regime we observe a significant enhancement in the wall shear stress attributed to an increment in particle stress and not the Reynolds stress. Examining the particle dynamics, particle distribution, dispersion, relative velocities and collision kernel, confirms the existence of the three regimes. We further study the transition and turbulence in the dilute regime of finite size particulate channel flow. We show that the turbulence can sustain in the domain at Reynolds numbers lower than the one of the unladen flow due to the disturbances induced by particles.

Descriptors: non-Newtonian flow, global stability analysis, inertial suspensions, particle dynamics

Stabilitetsanalys och inertial områden av komplexa fluider

Iman Lashgari
Linné Flow Centre, KTH Mekanik, Kungliga Tekniska Högskolan
100 44 Stockholm, Sweden

Abstrakt

I detta arbete studerar vi icke-newtonska effekter på tröghetsrelaterade instabiliteten i sjkuvflöden, samt så kallade *inertial suspensions*, d.v.s suspension vars rörelse är dominerad av tröghetskrafter. Vi studerar partiklar av finit storlek och arbetet är baserad på numeriska simuleringar.

I den första delen av arbetet undersöks både oelastiska (Carreau) och elastiska fluider (Oldroyd-B och FENE-P) för att förstå uppförandet av icke-newtonska fluider. Ett flertal klassiska strömningsfall som strömningen kring en cirkulär cylinder och i en så kallad *lid-driven* kavitet, samt kanalströmning har undersökts. Instabilitetsmekanismerna hos dessa fluider har undersökts med hjälp av modal och icke-modal stabilitetsanalys samt energi och känslighetsanalys. Studierna är baserade på linjär stabilitetsteori. Under inverkan av de icke-newtonska effekterna har betydande ändringar/förändringar i instabiliteten i de olika flödena observerats. Generellt, destabiliserar/stabiliserar skjuvningsförtunnande/skjuvningsförtjockande effekter strömningen runt cylindern och i kaviteten. Viskoelastiska effekter både stabiliserar och destabiliserar kanalströmningen, beroende på förhållandet mellan den viskoelastiska tidskalan och strömningens tidsskalor. Instabilitetsmekanismerna är bara marginellt modifierade i cylinderfallet medan nya instabilitetsmekanismer uppstår i fallet med lid-driven kavitet.

I den andra delen, använder vi direkt numeriska simuleringar tillsammans med den så kallad *Immersed Boundary* metoden för att simulera *inertial suspensions* av neutralflytande stela sfäriska partiklar i en kanal. Studierna omfattar en bredd skala av Reynoldstal, $500 \leq Re \leq 5000$, och partikelvolymsfraktion, $0 \leq \Phi \leq 0.3$. Här har vi hållit förhållandet mellan kanalhöjden och partikeldiameter, $2h/d = 10$, konstant. Tre olika områden har identifierats genom att studera spänning i tvåfasströmningar. Dessa områden är laminärt, turbulent och skjuvningsförtjockande där spänningar orsakade av viskositet, turbulens respektive partiklar bidrar mest i överföring av rörelsemängden inne i kanalen. Där skjuvningsförtjockande är dominant ser vi en betydande ökning av väggskjuvspänningen. Den kan tillskrivas en ökning i spänningen orsakad av partiklar och inte den turbulensen. Förekomsten av dessa områden har bekräftats genom analys av partiklarnas dynamik, fördelning, spridning, relativa hastigheter, samt kollision. Vidare studerar vi övergången från laminär till turbulent strömning för fall med låg partikelhalt. Vi visar att i dessa fall turbulensen kan vidhållas för ett lägre värde på Reynoldstalet än det för strömning utan partiklar. Detta beror på störningar som genereras av partiklar.

Descriptors: icke-newtonska fluider, global stabilitet analys, inertial suspensions, partikeldynamik

Preface

The current study focuses on the stability analysis of non-Newtonian fluids in different flow configurations and inertial flow regimes of suspension of finite size rigid particles in a channel. In the first part, we introduce the non-Newtonian models and tools for linear stability analysis which have been employed. In the second part, we review the suspensions of rigid particles and discuss their bulk behaviors in connection with the particle dynamics. The main findings of different studies have been summarised. In the third part, the following articles are presented.

Paper 1. I. Lashgari, J. O. Pralits, F. Giannetti & L. Brandt, 2012
First instability of the flow of shear-thinning and shear-thickening fluids past a circular cylinder.
J. Fluid Mech. **701**:201-227

Paper 2. S. Haque, I. Lashgari, F. Giannetti & L. Brandt, 2012
Stability of fluids with shear-dependent viscosity in the lid-driven cavity.
J. non-Newtonian Fluid Mech. **173-174**:49-61

Paper 3. M. Zhang, I. Lashgari, T. A. Zaki & L. Brandt, 2013
Linear stability analysis of channel flow of viscoelastic Oldroyd-B and FENE-P fluids.
J. Fluid Mech. **737**:249-270

Paper 4. I. Lashgari, O. Tammisola, V. Citro, M. P. Juniper & L. Brandt, 2014
The planar X-junction flow: stability analysis and control.
J. Fluid Mech. **753**:1-28

Paper 5. I. Lashgari, F. Picano, W.-P. Breugem & L. Brandt, 2014
Laminar, turbulent and inertial shear-thickening regimes in channel flow of neutrally buoyant particle suspensions.
Physical Review Letters. **113**:254502

Paper 6. I. Lashgari, F. Picano, W.-P. Breugem & L. Brandt, 2016
Channel flow of rigid sphere suspensions: Particle dynamics in the inertial regime.
International Journal of Multiphase Flow. **78**:12-24

Paper 7. I. Lashgari, F. Picano & L. Brandt, 2015
Transition and self-sustained turbulence in dilute suspensions of finite-size particles.
Theoretical and Applied Mechanics Letters. **5**:121-125

Division of work between authors
The research project was initiated by Prof. Luca Brandt (LB) as the main advisor.

Paper 1
The computations have been performed by Iman Lashgari (IL) using the codes developed by Flavio Giannetti (FG). The analyses have been done by IL with the help from Jan. O. Pralits (JP) and LB. The paper has been written by IL with feedback from JP, FG and LB.

Paper 2
The computations have been performed by Simon Haque (SH) using the codes developed by FG. The analyses have been done by SH and IL with the help from FG and LB. The paper has been written by SH and revised by IL with feedback from FG and LB.

Paper 3
The computations have been performed by Mangqi Zhang (MZ) using the codes developed by MZ. The analyses have been done by MZ and IL with the help from LB. The paper has been written by MZ with feedback from IL, Tamer Zaki and LB.

Paper 4
The computations have been performed by IL and Outi Tammisola (OT) using the code Nek5000 and the codes developed by Hugh Blackburn and Vincenzo Citro (VC). The analyses have been done by IL and OT. The paper has been written by IL and OT with feedback from VC, Matthew. P. Juniper and LB.

Paper 5
The computations have been performed by IL using the code developed by Wim-Paul Breugem (WB). The analyses have been done by IL and Francesco Picano (FP) with the help from LB. The paper has been written by IL with feedback from FP, WB and LB.

Paper 6
The computations have been performed by IL using the code developed by WB. The analyses have been done by IL with the help from FP and LB. The paper has been written by IL with feedback from FP, WB and LB.

Paper 7
The computations have been performed by IL using the code developed by WB. The analyses have been done by IL with the help from LB. The paper has been written by IL with feedback from FP and LB.

Part I

Global stability analysis of complex flows

CHAPTER 1

Introduction

Unlike pure water or oil, large variety of fluid flows are complex due to the presence of macromolecular structures dissolved/suspended in the fluid. Paints, polymer solutions, colloidal suspensions, gels and blood are some examples of rheologically complex fluids. These fluids often exhibit non-Newtonian behaviours where the relation between the applied shear and stress in the flow is no longer linear and instantaneous, opposite to the Newtonian fluids, and the flow motion is governed by a more sophisticated set of equations. Understanding the behaviours of the complex flows is of significant interest due their vast fundamental and industrial applications. Complex dynamics and unexpected patterns observed in the complex fluids under certain conditions have motivated many scientists with background in mathematics, physics, fluid mechanics, civil engineering, chemical engineering and biology to advance their knowledge about these fluids. In addition, many industrial processes such as food, chemical, plastic and polymer processing encounter the characteristics of the complex fluids.

The influence of the macromolecular structures on the flow system becomes more evident once they are perturbed under the action of an external shear. In the polymer solutions for example, the long chain polymer molecules tend to orient randomly at rest to obtain their minimum energy level (coil state). However, they respond to the external shear by disentangling and aligning in the flow direction (stretched state) and produce strong elastic force. This phenomenon has a significant impact on the behavior of the underlying flow (Deshpande *et al.* 2010). Adding small amount of high-molecular weight polymers to the fluid, the pressure force for driving the turbulent flow of polymeric solution at a fixed flow rate through a channel may decreases by 80% with respect to that for the Newtonian fluid (White & Mungal 2008). This area has been subjected to many studies since 50s and still is an ongoing research (see the early discovery by Toms (1949) and the review articles by Lumley (1973) and Procaccia *et al.* (2008)).

Non-Newtonian fluids may exhibit elasticity, memory effect, yield stress, shear-thinning, shear-thickening and etc under various circumstances. Elastic effects describe the tendency of the complex structures to relax back to their original configurations after being stretched by the flow (Renardy 1987). Memory effect has a close connection to the elasticity of the fluid. Flow may remember the history of its past deformation over a period identified by a

relaxation time (Bird *et al.* 1987; Deshpande *et al.* 2010). Fluids with yield stress start to flow if subject to an external stress which is larger than a certain threshold (e.g. Bingham fluids; see Phan-Thien 2002). Shear-thinning and shear-thickening fluids display an apparent viscosity which varies with the local shear-rate of the flow.

In the first part of the thesis, we focus on non-Newtonian effects on instability characteristics of the flow. Instabilities in non-Newtonian fluids may arises directly from the non-Newtonian character of the fluids and/or via a modification of the Newtonian fluids due to the non-Newtonian properties (Pearson 1976). The former effect has been mostly investigated in the context of the inertialess instabilities and the latter one has been examined in inertia-dominated flows. The phenomenon of elastic instability has been discovered in flows with negligible inertia and strong elastic force. It is believed that the nonlinear behavior of the complex structures in the flow provides a driving force to promote instabilities (Shaqfeh 1996). Development of these instabilities may results in elastic turbulence, a flow regime characterized by a wide range of temporal and spatial scales even at very low Reynolds numbers (Groisman & Steinberg 2001). The knowledge obtained from the study of elastic turbulence has been used in processes whose aim is to manipulate the flow at small scales, for example to enhance mixing in micro-fluidic devices (Larson 1992). It is also important to study the instability of non-Newtonian flows in the inertial regime. This area is in particularly relevant in various industrial processes such as lubrication, extrusion, coating and fibre spinning. Inertial flow might be stabilized or destabilized by non-Newtonian effects depending on the choice of the flow and rheological parameters (Tanner 1985). In these flows, the modification of the instability thresholds and/or alteration of the instability mechanisms is attributed to the interplay between inertial, viscous and elastic forces. To gain more insight into these effects, is the main motivation behind the first part of the current study.

In this part, a range of tools for the linear stability analysis are employed to investigate the dynamic of instabilities in inertial non-Newtonian fluids. We use modal analysis to assess the time-asymptotic behavior of the flow dynamics while the short time dynamics of the system is studied by means of nonmodal analysis. Sensitivity analysis, a measure of flow response to internal or external modifications, is used to indicate the region in the flow which contributes the most to the instability dynamics. Finally, we study the perturbation kinetic energy budget to examine the physical mechanism behind the instabilities.

The Part I of the thesis is organized as follow. In § 2, we introduce an inelastic and two elastic non-Newtonian models and the numerical methods employed in this work. In § 3, we establish the stability analysis formulations: modal, non-modal, sensitivity and energy analysis with particular attention on the non-Newtonian modifications.

CHAPTER 2

Non-Newtonian fluids

The physical and chemical properties of the non-Newtonian fluids cannot be easily modelled by studying the interactions between the macromolecular structures, because those interactions in many rheologically interesting systems are too complex. Alternatively the constitutive equations are established based on the continuum mechanics to predict the behaviour of the non-Newtonian fluids. The constitutive equations can be divided into inelastic and elastic models. In the inelastic models the focus is mainly on the instantaneous variation of the fluid viscosity by the shear; i.e. Power-law, Carreau and Bingham models. These models are relatively easy to be used in the analytical and numerical studies however, they cannot capture all the aspects of the non-Newtonian fluids such as elasticity and memory effects. In the elastic models the stress does not grow/decay instantaneously by applying/removing shear to account for the memory effect of the flow, i.e. Maxwell, Oldroyd-B and FENE-P models. To model the non-Newtonian fluids often the viscous and elastic effects are combined based on a similar principal as a mechanical system containing springs and dashpots (see Morrison 2001). Although the non-Newtonian models are idealized, they can capture the behavior of real fluids under specific conditions. In this work we employ the Carreau, Oldroyd-B and FENE-P models to investigate the shear-thinning, shear-thickening and viscoelastic aspects of non-Newtonian fluids in the framework of the linear stability analysis.

2.1. Governing equation

The Cauchy momentum and continuity equations govern the motion of the flow of both Newtonian and non-Newtonian fluids,

$$\frac{\partial \mathbf{u}}{\partial t} + \mathbf{u} \cdot \nabla \mathbf{u} = -\frac{1}{\rho}\nabla p + \frac{1}{\rho}\nabla \cdot \tau \qquad (2.1)$$
$$\nabla \cdot \mathbf{u} = 0,$$

where $\mathbf{u} = (u, v, w)$ is a vector containing velocity components, p is pressure, ρ is the constant density and τ is the deviatoric stress. The stress in the generalized Newtonian fluids (Deshpande *et al.* 2010) is a linear function of the instantaneous flow deformation rate and it is constructed by $\tau = \mu(\nabla \mathbf{u} + (\nabla \mathbf{u})^T)$, where the fluid viscosity, μ, is the coefficient of proportionality. If the viscosity is constant, the governing equation forms the classical Navier-Stokes equation for the Newtonian fluids. Otherwise, the generalized N-S equation is

obtained,

$$\frac{\partial \mathbf{u}}{\partial t} + \mathbf{u} \cdot \nabla \mathbf{u} = -\frac{1}{\rho}\nabla p + \frac{1}{\rho}\nabla[\mu(\nabla \mathbf{u} + (\nabla \mathbf{u})^T)]. \tag{2.2}$$

Equation 2.2 has been used to describe the motion of inelastic and time-independent non-Newtonian fluids. These fluids do not show memory of their past deformations and their viscosity may depend on the local deformation rate in the flow. In § 2.2 we introduce a model for the viscosity of inelastic fluids to close the system of the equations.

In general, non-Newtonian fluids may exhibit elasticity and time-dependency. The deviatoric stress of these fluids is a nonlinear function of the history of the flow deformations; it does not only follow the Newton's law of viscosity but also does not agree with Hooke's law of elasticity (Deshpande *et al.* 2010). This property leads to a more complicated equation of motion for the viscoelastic fluids which might be highly nonlinear even for parallel flows. In § 2.3 we present two constitutive equations to model the behavior of the viscoelastic fluids.

2.2. Inelastic model

In this work, we employ the Carreau law to define the viscosity of the inelastic fluids. The Carreau model fits well-enough to the viscosity data taken from most engineering calculations (Bird 1976). The model presents an isotropic viscosity which is a function of the instantaneous flow shear-rate,

$$\mu = \mu_\infty + [\mu_0 - \mu_\infty][1 + (\lambda\dot{\gamma})^2]^{(n-1)/2}. \tag{2.3}$$

The second invariant of the strain-rate tensor, $\dot{\gamma}$, is obtained by the dyadic product $\dot{\gamma} = (2\Theta_{ij} : \Theta_{ij})^{\frac{1}{2}}$, where $\Theta = \frac{1}{2}(\nabla \mathbf{u} + \nabla \mathbf{u}^T)$ (see Bird *et al.* 1987). The power index, n, categorizes the fluid. For $n < 1$, the fluid is shear-thinning (pseudoplastic) and the viscosity of the flow decreases monotonically with the shear-rate. For $n > 1$, the fluid is shear-thickening (dilatant) and the flow becomes more viscous by increasing the shear-rate. The power index, $n = 1$, represents the Newtonian fluids. The parameters μ_0 and μ_∞ indicate the upper and lower limits of the fluid viscosity at zero shear-rate and infinite shear-rate (for the shear-thinning fluid). The material time constant λ indicates the degree of shear-thinning/shear-thickening and its value can be connected to the molecular structure of some polymeric solutions (Morrison 2001).

Numerous studies consider the instability of inelastic non-Newtonian fluids where the authors have compared their results with the one of the Newtonian fluids. Since the viscosity of inelastic non-Newtonian fluids is not constant, the choice of the reference viscosity in the definition of the Reynolds number affects the results over different studies (see the recent review by Govindarajan & Sahu 2014). In channel flow of an inelastic fluid, Nouar *et al.* (2007) claim that the tangent viscosity, $\mu_t = d\tau_{xy}/d\dot{\gamma}_{xy}$, at the wall is more relevant choice for the reference viscosity than the average viscosity in the domain. However, in the open flows like flow past a cylinder, those choices are not useful because

flow is separating and the viscosity variation is localized near the cylinder. In the work by Lashgari *et al.* (2012) on the shear-thinning and shear-thickening flows past a cylinder, the instability thresholds have been obtained when the Reynolds number constructed by the zero shear-rate viscosity. It is shown that if the reference viscosity is defined as a weighted average of the local viscosity and the norm of the function describing the core of instability is used as the weight function, the critical Reynolds numbers for all the cases studied collapse at ≈ 47.

2.3. Viscoelastic models

Several models have been developed to capture the viscoelastic behavior, viscose responses and elasticity, of some non-Newtonian fluids such as dilute polymer solutions. Polymer solutions exhibit shear-thinning and elastic effect (Bird *et al.* 1987; Phan-Thien 2002; Deshpande *et al.* 2010). In the current work we employ Oldroyd-B and FENE-P models to describe the behavior of the viscoelastic fluids. Both models represents an individual polymer molecule as a dumbbell with two beads at each end connected with an elastic spring (Giesekus 1982; Zhu *et al.* 2012). Unlike Oldroyd-B, FENE-P model imposes a limit on the maximum extension of the polymer molecules. Polymer additive affects the fluid through an extra body stress, τ_p, defined by the following non-dimensional form

$$\tau_p = \frac{f\mathbf{C} - I}{W}. \tag{2.4}$$

In this expression $\mathbf{C}$ is the conformation tensor constructed by taking an average over the polymer configurations, $C_{ij} =< R_i R_j >$, where $\mathbf{R}$ is a vector connecting the end points of a polymer molecule. The Weissenberg number, W, is the ratio between the polymer relaxation time and the characteristics flow time scale. For small values of W, polymer molecules rapidly adjust to the variation of the surrounding flow. Therefore, flow does not exhibit strong viscoelastic effects. The opposite applies to high values of W when the polymer molecules have time to be stretched. The Peterlin function, f, is equal to one for Oldroyd-B fluids while it is

$$f = \frac{L^2 - 3}{L^2 - C_{kk}}, \tag{2.5}$$

for FENE-P fluids. In equation 2.5, L is the maximum extensibility of the polymer molecules and C_{kk} is the trace of the conformation tensor. Taking into account the polymer stress, the non-dimensional form of the governing equations reads

$$\frac{\partial \mathbf{u}}{\partial t} + \mathbf{u} \cdot \nabla \mathbf{u} = -\nabla p + \frac{\beta}{Re}\nabla^2 \mathbf{u} + \frac{1-\beta}{Re}\nabla \cdot \tau_p, \tag{2.6}$$

where β is the ratio between the solvent viscosity and the total viscosity of the fluid. Note that we use the same notation for the non-dimensional quantities as those of the dimensional in equations 2.1 and 2.2 . When β approaches one, the

contribution of the polymer stress is negligible. The Reynolds number is defined by $Re = UL/\nu$ where U and L are the characteristics velocity and length scale and ν is the total viscosity of the mixture. The constitutive equation for the evolution of the conformation tensor reads

$$\frac{\partial \mathbf{C}}{\partial t} + \mathbf{u} \cdot \nabla \mathbf{C} - \mathbf{C} \cdot \nabla \mathbf{u} - (\nabla \mathbf{u})^T \cdot \mathbf{C} = -\tau_p, \tag{2.7}$$

where T stands for transpose of the tensor. The left hand side of equation 2.7 is the upper convective time derivative (Maxwell derivative) which indicates the transport and stretch of the polymer molecules. This is balanced by the polymer stress in the constitutive equation.

2.4. Numerical methods

In this part we briefly discuss the numerical methods which have been used in the first part of the thesis.

2.4.1. *CPL code*

The numerical code employed in **paper 1** and **paper 2** is a modified version of the second order finite difference code described in Giannetti & Luchini (2007). In the first step the base flow is computed by solving the non-linear steady Navier-Stokes equations via Newton-Raphson iterations. The base flow solution is then inserted into the perturbation equations where the eigenvalues and eigenmodes of the linearized stability problem are computed via the Arnoldi algorithm with a shift and invert strategy. The adjoint modes are obtained as left eigenvectors of the discrete problem. The resulting eigenvalues of the adjoint problem are equal to those of the direct mode to machine precision. Finally the core of the instability is obtained by multiplying the direct and adjoint fields. Note that the linearized and the sensitivity equations are given in § 3.

The spatial derivatives are computed on the staggered grids using the classical central differences and the time integration scheme adopted for the stability analysis is the Crank-Nicolson method. In order to obtain more accurate results, both the base flow and the stability problem have been discretized on a smoothly varying stretched grid, with computational nodes clustered near the cylinder in **paper 1** and near the cavity wall in **paper 2**. The presence of the cylinder is captured using an Immersed Boundary technique where the velocities at the grid points near the cylinder surface are forced to those values needed to fulfil the zero velocity condition on the surface by interpolation.

2.4.2. *Spectral code*

In **paper 3** we use a spectral stability solver to perform the stability analysis of the polymeric flow in a channel. In spectral method the solution is expanded using a set of ansatz functions. The scheme is global due to the global nature of those ansatz functions opposite to the finite-difference method where the information at each point only depends on the neighbouring points. The spectral

method gives the exponential converges of error by increasing the number of grid points.

The original stability solver is a spectral collocation method formulated using the wall normal velocity, v, and vorticity, η (see for example Schmid & Brandt 2014). The equations are discretised on Chebyshev points employing Chebyshev polynomials, $L_j(y)$, where y is the wall normal coordinate. The use of the Chebyshev points provides higher resolution close to the walls where shear is the strongest. The Chebyshev polynomials are modified using a pre-factor to account for the boundary conditions on the bottom and top walls of the channel,

$$L_j^+(y) = (\frac{1-y^2}{1-y_j^2})^2 L_j(y), \tag{2.8}$$
$$L_j^+(y) = (\frac{1-y^2}{1-y_j^2}) L_j(y).$$

These pre-factors correspond to the the Orr-Sommerfeld and Squire problems respectively. At the first step the steady solution of the governing equations (base flow) is obtained analytically. The base flow for the FENE-P model slightly differs from the parabolic profile as shown in **paper 3**. The base flow is then given to the stability solver as an input. The linear system is modified by including the components of the conformation tensor in the perturbation vector, i.e. $\phi = (v, \eta, c_{11}, c_{22}, c_{33}, c_{12}, c_{13}, c_{23})^T$. The corresponding linearised matrixes are then expanded to the size of $(8N+12) \times (8N+12)$, where v and η are approximated by N modes whereas each component of the conformation tensor c_{ij} is approximated by $N+2$ modes.

2.4.3. *Nek5000 and DOG codes*

We employ spectral element code, nek5000 (see Tufo & Fischer 1999), to perform Direct Numerical Simulations in **paper 4**. In the Spectral Element Method, SEM, the computational domain is divided into quadrilateral spectral elements. Within each local element the solution is expanded using N^{th}-order Lagrange polynomial interpolants on Gauss-Lobatto-Legendre (GLL) quadrature points for the velocity space and $(N-2)^{th}$-order Lagrange interpolants on Gauss-Legendre (GL) points for the pressure. The scheme is therefore known as $\mathbb{P}_N - \mathbb{P}_{N-2}$ discretization following Maday & Patera (1989) which avoids spurious pressure fluctuations. The GLL distribution is a common choice for the Chebyshev and Lagrange polynomials which avoids the Runge phenomenon by clustering the points close to the boundary of each element. SME allows the simulations on the complex geometries while preserving the spectral accuracy of the method.

In Nek5000 the weak formulation of the governing equations is formed by multiplying Navier-Stokes equation with a test function and integrating the result in the physical space. The Galerkin method is implemented where the test

functions is chosen the same as the ansatz functions (Lagrange polynomials). Nek5000 exhibits an exponential convergence of the solution when the polynomial order is increased, p-refinement (see Patera 1984). It can also be used for localized refinement by increasing the number of elements, h-refinement. The viscous term is treated implicitly by 3^{rd}-order backward difference whereas the nonlinear terms are discretised by an explicit 2^{nd}-order extrapolation. Computing the nonlinear terms involve the expansions up to order $2N$. If the number of computational points is considered the same as the number of GLL points in an element, N, the truncation leads to aliasing error. To remove this error the over-integration is used where at least $3N/2$ points are taken into account. In addition a filtering method is employed to damp the highest order modes and avoid the numerical instabilities (see for more details Mullen 2001). Nek5000 is massively parallelised and scalable to thousands cores which makes it an attractive choice for the large simulations of the flow in complex configurations.

In **paper 4** we also use the stability solver, DOG, (Barkley *et al.* 2008). DOG is derived from the nonlinear solver, Semtex, where the nonlinear terms are modified and additional routines are included to solve the eigenvalues of the system. The nonlinear terms are treated explicitly and the Stokes operator is inverted using the velocity correction technique. DOG is employed to perform three-dimensional stability analysis about the two-dimensional base flows. It solves the perturbation fields in Fourier-transformed space by a time stepping technique. The eigen-solution of the stability problem is obtained by an standard orthogonal projection of the linear operator onto the low-dimensional Krylov subspace and using a built-in library, together with ARPACK.

CHAPTER 3

Global linear stability and sensitivity analysis

In this chapter we briefly outline the tools that have been used to study the instabilities in inertial non-Newtonian flows.

3.1. Linear analysis

Linear stability analysis provides an appropriate explanation for the instability phenomena observed in the early stage of the transition from laminar to turbulent flow. To perform a linear stability analysis, we decompose the flow variables into the steady base flow variables $(\mathbf{U}_b, P_b, \mu_b, C_b, f_b, \tau_{pb})$ and infinitesimal perturbations $(\mathbf{u}', p', \mu', c', f', \tau_p')$ and study the spatial and temporal evolution of the perturbations. Substituting the decomposition into the governing equations and neglecting the higher order terms, we obtain the Linearized Perturbation Equation (LPE). For the flow with shear-dependent viscosity, the LPE reads

$$\frac{\partial \mathbf{u}'}{\partial t} + \mathbf{u}' \cdot \nabla \mathbf{U}_b + \mathbf{U}_b \cdot \nabla \mathbf{u}' = -\nabla p' + \tag{3.1}$$
$$\frac{1}{Re}\nabla \cdot [\mu_b(\nabla \mathbf{u}' + (\nabla \mathbf{u}')^T) + \frac{1}{Re}\nabla \cdot [\mu'(\nabla \mathbf{U}_b + (\nabla \mathbf{U}_b)^T),$$
$$\nabla \cdot \mathbf{u}' = 0.$$

We define the viscosity fluctuation, μ', by the linear term of the Taylor expansion of the viscosity function around the base state,

$$\mu' = \dot{\gamma}_{ij}(\mathbf{u}')\frac{\partial \mu}{\partial \dot{\gamma}_{ij}}(\mathbf{U}_b). \tag{3.2}$$

Equation 3.1 has been adopted for the parallel flows of fluids with varying viscosity where the formulation of the modified Orr-Sommerfeld operator are presented in the works by Chikkadi *et al.* (2005) and Nouar *et al.* (2007).

The LPE and linearized constitutive equation for the polymeric flows reads

$$\frac{\partial \mathbf{u}'}{\partial t} + \mathbf{U}_b \cdot \nabla \mathbf{u}' + \mathbf{u}' \cdot \nabla \mathbf{U}_b = -\nabla p' + \frac{\beta}{Re}\nabla^2 \mathbf{u}' + \frac{1-\beta}{Re}\nabla \cdot \tau_p' \tag{3.3}$$
$$\frac{\partial \mathbf{c}'}{\partial t} + \mathbf{u}' \cdot \nabla \mathbf{C}_b + \mathbf{U}_b \cdot \nabla \mathbf{c}' - \mathbf{c}' \cdot \nabla \mathbf{U}_b - \mathbf{C}_b \cdot \nabla \mathbf{u}' - (\nabla \mathbf{U}_b)^T \cdot \mathbf{c}'$$
$$-(\nabla \mathbf{u}')^T \cdot \mathbf{C}_b = -\tau_p', \tag{3.4}$$

where $\tau_p' = \frac{f'\mathbf{C}_b + f_b\mathbf{c}'}{W}$. The perturbation of the Peterlin function, f', is obtained by Taylor expansion in the same manner,

$$f' = \frac{\partial f}{\partial C_{11}}\Big|_B c_{11} + \frac{\partial f}{\partial C_{22}}\Big|_B c_{22} + \frac{\partial f}{\partial C_{33}}\Big|_B c_{33}, \tag{3.5}$$

where $\big|_B$ shows that the derivatives are taken from base flow variables.

The LPE for both inelastic and elastic cases can be written as

$$\frac{\partial \mathbf{q}'}{\partial t} = \mathbf{L}(\mathbf{Q}_b, Re)\mathbf{q}', \tag{3.6}$$

where $\mathbf{Q}_b$ and $\mathbf{q}'$ represent the base flow and perturbation variables and $\mathbf{L}$ denotes the linear operator.

3.2. Modal analysis

In parallel flows, where the velocity profile of the base flow is a function of just the wall-normal coordinate, Fourier decomposition of the perturbations can be performed in both streamwise and spanwise directions. The decomposition reads

$$\mathbf{q}'(x, y, z, t) = \hat{\mathbf{q}}(y) exp(\sigma t + i\alpha x + i\gamma z), \tag{3.7}$$

where α and γ are the streamwise and spanwise wavenumbers introduced to exploit the homogeneity of the base flow in the streamwise and spanwise directions. The eigenvalue and eigenvectors of the global modes are σ and $\hat{\mathbf{q}}$. The real and imaginary part of σ are the growth rate and oscillation frequency of the each mode. The above procedure is a basis of the local instability analysis which can be also applied in the weakly non-parallel flows where the variation of the base flow occurs over a much larger length scale than the wavelength of the perturbations (Huerre & Monkewitz 1990).

When the flow is highly non-parallel, the stability analysis has to be fulfilled globally in the entire domain. In the first part of the thesis we investigate the evolution of the three-dimensional perturbations on the two dimensional steady base flows (except for the channel flow). Following the terminology in Theofilis (2011), we perform BiGlobal stability analysis where the global modes evolve exponentially in time,

$$\mathbf{q}'(x, y, z, t) = \hat{\mathbf{q}}(x, y) exp(\sigma t + i\gamma z). \tag{3.8}$$

Introducing equation (3.8) into (3.6), we form the Linearized Eigenvalue Problem (LEP) to compute the eigenvalues and eigenvectors of the system,

$$\sigma\hat{\mathbf{q}} = \mathbf{L}(\mathbf{Q}_b, Re)\hat{\mathbf{q}}. \tag{3.9}$$

If there exists any eigenvalue with $\Re\{\sigma\} > 0$, the flow is linearly unstable. Conversely, if all the eigenvalues have negative real part the infinitesimal perturbations eventually decay to zero and flow is linearly stable.

3.3. Nonmodal analysis

Even though modal stability analysis predicts a critical Reynolds number above which the perturbations grow exponentially, in the experiments, flows may undergo transition to turbulence at much lower Reynolds numbers. In these conditions the dynamics of the system may not be determined by the least stable eigenvalue whereas the superposition of stable modes results in a transient amplification of the energy owing to the non-orthogonality of the eigensystem (Schmid & Henningson 2001). If the growth is large enough, nonlinear interactions may trigger the transition from laminar to turbulent flow. Transient growth of the energy has been observed in many open flows and it is in particular more evident in the spatially varying flows where convective term in N-S equation is highly asymmetric (Barkley *et al.* 2008).

Transient growth analysis gives the maximum amplification of the kinetic energy, at a finite time horizon T, over the all permissible initial perturbations (Schmid 2007). The optimal growth is defined by

$$G(T) = \underset{\mathbf{q}'(0)}{max} \frac{E(\mathbf{q}'(T))}{E(\mathbf{q}'(0))}, \tag{3.10}$$

where $\mathbf{q}'(0)$ and $\mathbf{q}'(T)$ are the optimal initial and final conditions and E is the perturbation kinetic energy obtained by the standard L_2 inner product, $E(t) = (\mathbf{q}'(t), \mathbf{q}'(t))$. The energy growth forms

$$G(T) = \frac{(\mathbf{q}'(T), \mathbf{q}'(T))}{(\mathbf{q}'(0), \mathbf{q}'(0))} = \frac{(exp(\mathbf{L}T)\mathbf{u}'(0), exp(\mathbf{L}T)\mathbf{u}'(0))}{(\mathbf{u}'(0), \mathbf{u}'(0))} = \tag{3.11}$$

$$\frac{(\mathbf{A}(T)\mathbf{u}'(0), \mathbf{A}(T)\mathbf{u}'(0))}{(\mathbf{u}'(0), \mathbf{u}'(0))},$$

where $\mathbf{A}(T) = exp(\mathbf{L}T)$, is the propagator operator (Farrell & Ioannou 1996). The adjoint of the propagator operator, $\mathbf{A}^+(T)$, necessarily satisfies the following correlation for any fields $\hat{\mathbf{a}}$ and $\hat{\mathbf{a}}^+$,

$$(\mathbf{A}(T)\hat{\mathbf{a}}, \hat{\mathbf{a}}^+) = (\hat{\mathbf{a}}, \mathbf{A}^+(T)\hat{\mathbf{a}}^+). \tag{3.12}$$

Combining equations 3.11 and 3.12, the optimal growth reads

$$G(T) = \frac{(\mathbf{u}'(0), \mathbf{A}^+(T)\mathbf{A}(T)\mathbf{u}'(0))}{(\mathbf{u}'(0), \mathbf{u}'(0))}. \tag{3.13}$$

Based on the above expression, the leading eigenvalue of the product operator $\mathbf{A}^+(T)\mathbf{A}(T)$ (the largest singular value of $\mathbf{A}$) indicates the maximum amplification of the perturbation kinetic energy over the time horizon T. A sequence of propagating an initial condition forward in time by the direct operator, $\mathbf{A}(T)$, and backward in time by the adjoint operator, $\mathbf{A}^+(T)$, results in the optimal initial condition which exhibits the maximum growth over the optimization time (Adjoint looping). The structure of the optimal mode and

the time scale over which the optimal mode affects the flow are significantly different than the ones of the global modes (Schmid 2007).

In this work we will show that the non-Newtonian properties of flow may affect both modal and non modal instabilities by drifting global modes to the other side of the complex plane and through a modification of the transient growth process.

3.4. Sensitivity analysis

Sensitivity analysis has been introduced to measure the sensitivity of the fluid system to different internal or external modifications such as structural, base flow, boundary velocity and body geometry modifications (Chomaz 2005; Giannetti & Luchini 2007). It can be used to specify region/s in the flow that contribute the most to the dynamics of the system. The knowledge obtained from the sensitivity analysis can be therefore employed to control the flow by manipulating the sensitive regions.

To compute the sensitivity function, we design a constrained optimization problem where the cost function is the eigenvalue of the system and the constrains are LEP and the governing equation for the base flow (Marquet *et al.* 2008). We then employ the generalized Lagrange identity to construct an unconstrained optimization problem by introducing the adjoint perturbation and base flow variables ($\hat{\mathbf{q}}^+$, $\mathbf{Q}_b^+$) as the Lagrange multipliers,

$$\Upsilon = \sigma - (\hat{\mathbf{q}}^+, LEP\{\hat{\mathbf{q}}, \mathbf{Q}_b, \sigma, \hat{\mathbf{f}}\}) - (\mathbf{Q}_b^+, BF\{\mathbf{Q}_b, \mathbf{F}\}). \tag{3.14}$$

In this expression Υ is the Lagrangian function and BF stands for the base flow equation. The parameters $\hat{\mathbf{f}}$ and $\mathbf{F}$ denote the possible forcing on perturbation and base flow equations respectively. The governing equations for the adjoint perturbation and adjoint base flow variables are obtained by $\frac{\partial \Upsilon}{\partial \hat{\mathbf{q}}} = 0$ and $\frac{\partial \Upsilon}{\partial \mathbf{Q}_b} = 0$ (Gunzburger 2003). The structure of the adjoint variables are not only useful to compute the sensitivity functions but also valuable on its own right. The spatial structure of the adjoint perturbation mode indicates the region/s in the flow where the receptivity to the external excitations at perturbation level is the highest. The structure of the adjoint base flow presents the sensitivity of the flow to steady forcing at base flow level (see for more details Marquet *et al.* 2008; Luchini & Bottaro 2014).

Note that the transient growth analysis in § 3.3 is also an optimization problem in which the maximum amplification of the perturbation kinetic energy serves as the cost function and the constraints are the LPE and the energy of the initial conditions. Therefore, transient growth analysis can be seen as a sensitivity measure to initial condition (Schmid 2007).

3.4.1. *Structural sensitivity analysis*

In the flow systems, where the evolution operator is non-normal, there exists a large spatial separation between the structure of the global direct and

adjoint modes and dynamic of the system can not be determined by study either of them separately. Structural sensitivity function is then constructed by overlapping the direct and adjoint global modes, (Giannetti & Luchini 2007). Structural sensitivity analysis indicates the core of the instability (wave-maker region) where the structural modification of the system, in the form of local feedback force proportional to perturbation velocity, produces the largest drift in the eigenvalues. The dynamics of the system may promote a self-sustained mechanism in the wave-maker region. Indeed, the area outside the wavemaker region is insensitive to the structural modification of the flow and the dynamics of the system remain unchanged by removing this area from the computational domain (Chomaz 2005).

To compute the structural sensitivity, we assume the forcing on the LEP in the form of localized structural force proportional to local velocity perturbation, $\hat{\mathbf{f}} = \delta(x - x_0, y - y_0)\delta\mathbf{M}_0 \cdot \hat{\mathbf{u}}$, where $\delta\mathbf{M}_0$ is a coupling matrix of particular localized structure and δ is the Kronecker delta function (Giannetti & Luchini 2007). The governing equation for the eigenvalue drift is obtained by using the expansion $\hat{\mathbf{q}} = \bar{\mathbf{q}} + \delta\hat{\mathbf{q}}$ and $\sigma = \bar{\sigma} + \delta\sigma$ in equation 3.9, where overbar stands for unperturbed variables,

$$\bar{\sigma}\delta\hat{\mathbf{q}} - \mathbf{L}(\mathbf{Q}_b, Re)\delta\hat{\mathbf{q}} = -\delta\sigma\hat{\mathbf{u}} + \delta\mathbf{M}_0 \cdot \hat{\mathbf{u}}. \tag{3.15}$$

Replacing equation 3.15 by LEP in the optimization problem (eq 3.14), the eigenvalue drift due to the local feedback reads

$$\delta\sigma(x_0, y_0) = \frac{\hat{\mathbf{u}}^+(x_0, y_0) \cdot \delta\mathbf{M}_0 \cdot \hat{\mathbf{u}}(x_0, y_0)}{\int_D \hat{\mathbf{u}}^+ \cdot \hat{\mathbf{u}} dA}. = \mathbf{S}(x_0, y_0) \cdot \delta\mathbf{M}_0. \tag{3.16}$$

We obtain the sensitivity map by the use of spectral norm of the sensitivity tensor, $\mathbf{S}$, which gives rise to the maximum possible coupling between the velocity components.

The derivations of the governing equations for global direct and adjoint mode as well as structural sensitivity function for the fluids with shear dependent viscosity has been detailed in Lashgari *et al.* (2012) and Haque *et al.* (2012).

3.4.2. *Sensitivity analysis to base flow modification*

Sensitivity analysis to generic base flow modifications, $\mathbf{S}_{BF}$, has been used to examine the variation of the eigenvalue of the system to small modifications in the base flow. Opposite to the structural sensitivity analysis, here the focus is on the variations in the base flow that strongly affect the instability dynamics. It is shown by Marquet *et al.* (2008) and Pralits *et al.* (2010) that the sensitivity to base flow modification for the flow past a stationary and rotating cylinder specifies the regions where the dynamics of the system contribute to the onset of vortex shedding. The response of the flow system to specific modifications in the

baseflow suggests the strategies for manipulating/controlling the instabilities in the flow.

To compute the sensitivity to the generic (arbitrary) base flow modification, we remove the base flow equation from the optimization problem (eq 3.14) and obtain the variation of the eigenvalue by $\frac{\partial \Upsilon}{\partial \mathbf{Q}_b} = 0$. Following the formulation in Marquet *et al.* (2008), the sensitivity to base flow modification is obtained by

$$\mathbf{S}_{BF} = \nabla_{\mathbf{Q}_b}\sigma = \frac{-(\nabla\hat{\mathbf{u}})^H \cdot \hat{\mathbf{u}}^* + \nabla\hat{\mathbf{u}}^+ \cdot \hat{\mathbf{u}}^*}{\int_D \hat{\mathbf{u}}^+ \cdot \hat{\mathbf{u}} dA}, \tag{3.17}$$

where * and ^{H} denote as complex conjugate and trans conjugate respectively.

3.4.3. *Sensitivity analysis to boundary velocity modification*

The optimization problem (eq 3.14) can be adopted when specific sensitivity analysis is desirable. As an example, the continuity equation can be explicitly included in the optimization problem as a constrain where the adjoint pressure serves as a Lagrange multiplier. Consequently the structure of the adjoint pressure indicates the region/s in the flow which is highly receptive to mass injection.

In **paper 4**, we have employed the sensitivity analysis to boundary velocity modification to obtain the optimal distribution of suction/blowing at the wall. Following the formulation introduced in Marquet & Sipp (2010), the sensitivity to boundary velocity modification, $\mathbf{S}_b$, is derived by adding a new constrain to the optimization problem (equation 3.14) corresponding to the boundary condition and defining the boundary velocity, $\mathbf{U}_B$, as the control parameter. The sensitivity function then reads

$$\mathbf{S}_b = \nabla_{\mathbf{U}_B}\sigma = P^+\mathbf{n} + Re^{-1}\nabla\mathbf{U}^+ \cdot \mathbf{n}, \tag{3.18}$$

where $\mathbf{U}^+$ and P^+ are the adjoint base flow velocity and pressure and $\mathbf{n}$ is a unit vector normal to the wall. The variation of the eigenvalues is then obtained by integrating $\mathbf{S}_B$ over the boundary B:

$$\delta\sigma = \int_B \mathbf{S}_b \cdot \delta\mathbf{U}_B. \tag{3.19}$$

3.5. Energy analysis

The perturbation kinetic energy analysis is a powerful tool to examine the physical mechanisms behind the instabilities. This method has been introduced long time ago and is still presented in the recent studies of both Newtonian and non-Newtonian fluids (Lanzerstorfer & Kuhlmann 2012; Doering *et al.* 2006). A more detailed aspects of the perturbation energy budget is presented in the book by Drazin (2002).

In this section, we introduce the perturbation kinetic energy budget for the non-Newtonian fluids. Since the velocity fluctuations are complex functions

(see 3.8), the evolution equation for disturbance kinetic energy is obtained by multiplying the LPE with complex conjugate of the velocity fluctuations, $u_i'^*$. For the fluids with shear dependent viscosity, the budget reads

$$\frac{d(e)}{dt} = \frac{\partial}{\partial x_j}\big[-\frac{1}{2}U_{bj}u_i'u_i'^* - \frac{1}{2}(u_j'^*p' + u_j'p'^*) + \frac{1}{Re}\mu_b(u_i'^*\theta_{ij} + u_i'\theta_{ij}^*) + \frac{1}{Re}\Theta_{ij}(u_i'^*\mu' + u_i'\mu'^*)\big] - \frac{1}{2}(u_i'^*u_j' + u_i'u_j'^*)\frac{\partial U_{bi}}{\partial x_j} - \frac{2}{Re}\mu_b(\theta_{ij}\theta_{ij}^*) - \frac{1}{Re}(\mu'\theta_{ij}^*\Theta_{ij} + \mu'^*\theta_{ij}\Theta_{ij}), \quad (3.20)$$

where $e = \frac{1}{2}(u_i'u_i'^*)$ is the perturbation kinetic energy and Θ_{ij} and θ_{ij} are the shear-rate tensors corresponding to baseflow and perturbation velocity fields. In the above expression * denotes the complex conjugate. The first term on the right hand side of the equation 3.20 corresponds to the transport of the energy in the domain and its overall contribution in the energy budget is zero in the flow system with vanishing perturbations at the boundaries. Note that this term is locally non-zero and can affect the energy budget indirectly by modifying the other terms (Govindarajan & Sahu 2014). The second term is the production of perturbation kinetic energy by means of Reynolds stress. The third term is viscous dissipation which is always negative. The last term results from the contribution of the viscosity fluctuation. As shown in Lashgari *et al.* (2012) for Carreau model, the last term is positive for the shear-thinning and negative for the shear-thickening fluids. Therefore, viscosity fluctuation in shear-dependent viscosity fluids contributes in destabilizing the flow by adding production and stabilizing the flow by increasing the dissipation.

The kinetic energy budget for the viscoelastic fluids is obtained by

$$\frac{\partial(e)}{\partial t} = \frac{\partial}{\partial x_j}\big[\frac{1}{2}U_{bj}u_i'u_i'^* - \frac{1}{2}(u_j'^*p' + u_j'p'^*) + \frac{\beta}{2Re}(u_i'^*\frac{\partial u_i'}{\partial x_j} + u_i'\frac{\partial u_i'^*}{\partial x_j}) + \frac{1-\beta}{2Re}(u_i'^*\tau_{pij}' + u_i'\tau_{pij}'^*)\big] - \frac{1}{2}(u_i'^*u_j'\frac{\partial U_{bi}}{\partial x_j} + u_i'u_j'^*\frac{\partial U_{bi}}{\partial x_j}) - \frac{\beta}{Re}\frac{\partial u_i'^*}{\partial x_j}\frac{\partial u_i'}{\partial x_j} - \frac{1-\beta}{2Re}(\tau_{pij}'\frac{\partial u_i'^*}{\partial x_j} + \tau_{pij}'^*\frac{\partial u_i'}{\partial x_j}), \quad (3.21)$$

where the last term on the right hand side, denoted as PD in **paper 3**, describes the interaction between the polymer stress and the the velocity fluctuations.

Perturbation kinetic energy directly connects to the growth rate of the global modes. The normalized rate of energy by the kinetic energy of the mode gives

$$\frac{\frac{\partial(e)}{\partial t}}{e} = 2\sigma_r, \tag{3.22}$$

where σ_r is the growth rate of the eigenvalue whose eigenfunction is employed to obtain the energy budget. Therefore, energy analysis can be used to examine the results of the stability analysis.

Part II

Inertial suspension of finite size rigid particles

CHAPTER 4

Particle suspensions

As mentioned in Part I, the presence of any kind of macromolecular particles suspended in a Newtonian fluid induces complex behaviour of the mixture. Particle suspensions can be found almost everywhere from natural and geophysical to biological and industrial flows. Pyroclastic flows in mountain, sedimentation flows in river bed, cloud and planetary flows are only few examples of the suspensions in nature. In biology, the motion of the red blood cells in a vessel is important for the material transport through the body. In industry suspensions are employed to facilitate the transportation and mixing of the particles through the carrier fluid such as flows in fluidised bed and hopper dredger. This broad range of applications motivates many scientists to study the behaviour of the suspensions form both macroscopic and microscopic point of views.

The complication in dealing with the suspensions stems from the fact that we are no longer solving a single phase but at least a two-phase flow problem. This requires to not only solve the governing equations of the carrier (continuum) phase, often Navier-Stokes and continuity equations, but also those of the particle (dispersed) phase as well as the conditional equations at the interface between the two phases. The difficulties are not limited to this level, because unlike the carrier phase often characterised by a single dimensionless parameter, the Reynolds number, solid phase depends on many parameters such as particle size, shape, volume fraction, deformability and density. This makes the problem of particle suspension multidimensional.

From the macroscopic point of view, suspending few particles in a Newtonian fluid induces non-Newtonian effects. As an example the mixture viscosity is no longer an intrinsic material property and depends on the applied shear rate (Brown & Jaeger 2014). Particle suspensions exhibit almost all the aspects of the non-Newtonian fluids from shear-thinning and shear-thickening to memory effect, yield stress and normal stress differences (Brady & Bossis 1985). These aspects are directly related to the rate of applied shear (Jeffrey & Acrivos 1976). The main reason to study the suspensions is to understand their macroscopic properties such as sedimentation rate, self diffusion, aggregation or in general rheology by connecting those behaviours to the microstructures in the mixture. The location, motion and properties of the particles and the surrounding fluids induce the macroscopic behaviour of the suspension (Brady & Bossis 1988).

As mentioned many parameters are to be considered to characterise a suspension. In the present work we restrict our focus on the inertial suspensions of finite size rigid and spherical neutrally buoyant particles. By inertial suspension we mean that inertia exists not only at bulk level but also at particle scale: i.e. particle Reynolds number, $Re_p = Ua/\nu$, where U is the characteristic fluid velocity, ν is the fluid kinematic viscosity and a is the particle radius, is not small. Note that there might be a flow case with large separation of scales, like blood flow in a large vessel, where inertia may presence at macro-scale but not at the scale of red blood cells (Koch & Hill 2001). In our study the typical particle size is much larger than the smallest scale in the flow; suspensions are non-colloidal and Brownian motion does not influence the particle motion. This condition exists in many applications like slurry transport where the typical particle size is between 100 to 1000 micron much larger than the size of the colloidal particles, about 1 micron (Jeffrey & Acrivos 1976). By employing neutrally buoyant particles we ensure that the role of inertia is isolated and results are realisable in experiment in the presence of gravity (Kulkarni & Morris 2008).

In particle suspensions different level of interactions may exist depending on the particle relaxation time, τ_p, and particle volume and mass concentration (Elghobashi 1994). The particle volume fraction, i.e. fraction of the total computational volume occupied by the particles, is denoted by Φ throughout the thesis. When the suspension is dilute, $\Phi \leq 10^{-6}$, the interaction between the particles and flow is regarded as one-way coupling. This implies that particles are just transported and do not influence the carrier fluid. When the particle volume fraction increases, i.e. $10^{-6} \leq \Phi \leq 10^{-3}$, the mass load of the dispersed phase becomes comparable with the one of the fluid phase and the regime is two-way coupling (Balachandar & Eaton 2010). In the two-way coupling regime the effects of the particles on the fluid should be taken into account whereas the inter-particle interactions are still negligible. At higher volume fractions, $\Phi \geq 10^{-3}$, we are in the dense regime where all the phases are mutually interact; i.e. four-way coupling. In this regime both hydrodynamic and contact interactions play an important role in the dynamics (Boyer *et al.* 2011). The effect of the inter-particle interactions becomes even more important when particle relaxation time increases. As reported by Elghobashi (1994) even at $\Phi \leq 10^{-3}$ the regime can be considered as four-way coupling at large values of τ_p. The relevant example for the regime of four-way coupling is the suspension of finite size particle at moderate or high values of the particle concentration which is the subject of the present study.

The suspension dynamics can be also categorised in five groups based on the particle size as proposed by Brady & Bossis (1988): 1) Molecular dynamics where the particle interactions are at atomic or molecular scale through a central force. 2) Macromolecular dynamics where big molecules like protein and polymer can be deformed and fold by the flow. 3) Stokesian dynamics where large colloidal particles dispersed in a continuum solver in which Van Der Waals

and Brownian forces are non-negligible. 4) Granular dynamics such as flowing sand and suspensions of large particles in fluids. 5) Gravitational or stellar dynamics where the interactions between the galaxies and stars takes place in vacuum following Newton's law of gravity. Considering these groups, the most complicated problem is the suspension of particles in the fluid where we deal with continuum medium opposite to the molecular and gravitational dynamics, fluid-particle interactions are important opposite to the granular flow and Reynolds number is not zero opposite the Stockesian dynamics.

In many numerical studies the point particle approximation is employed instead of resolving the flow around each particle, mainly due to computational limit. The point particle approximation is used where the variation in the interface between the dispersed and continuum phases is insignificant (Balachandar & Eaton 2010). The force applied on a particle is modelled analytically and contains terms corresponding to particle acceleration, added mass, Stokes drag, Basset history and gravity force (see Maxey & Riley 1983). The model is modified by Kim *et al.* (1998) to estimate more accurately the motion of spherical particles in unsteady flow for a range of particle Reynolds number from 2 to 150. In many applications the volume fraction of dispersed phase is high and/or the particle size is large with respect to the smallest scale in the flow such that the point particle approximation is no longer valid and fully resolved simulation of flow around an individual particle is needed. As the early attempts fully resolved simulation of a single particle is performed by Burton & Eaton (2005) in homogenous isotropic turbulence where they show that in the standard drag formula the contribution of the steady viscous drag is dominating and history term is negligible. Similar result is obtained by Bagchi & Balachandar (2003) when the particle is subjected to a frozen isotropic turbulent flow. In wall bounded turbulent flow, Zeng *et al.* (2009) study the drag force on a single spherical particle employing a spectral element method and a body-fitted mesh around the sphere. They report that the standard drag formulation for a single particle is valid only if the particle diameter is smaller than a certain threshold.

In the Part *II* of the thesis we use Direct Numerical Simulation together with an Immersed Boundary Method to simulate the inertial suspension of finite size particles in a broad range of Reynolds numbers and particle volume fractions. This part is organised as follows. In § 5 we discuss the governing equations and numerical method used to simulate the suspension of finite size particles. In § 6 we review transition and turbulence in the wall bounded flows of finite size particles. In § 7 we report the bulk quantities in the suspension, in particular the stress budget and effective viscosity. Finally in § 8 we discuss the particle dynamics focusing on particle distribution, dispersion and collision.

CHAPTER 5

Governing equations and numerical method

In this chapter we report the governing equations for the suspension of finite size particles. We then continue with the numerical approaches to attack this problem and finally we discuss the Immersed Boundary Method (IBM) which is used in the present work.

5.1. Governing equation

We study flow of finite size rigid particles suspended in a Newtonian fluid. The governing equations for the fluid phase are Navier-Stokes and continuity equations,

$$\rho(\frac{\partial \mathbf{u}}{\partial t} + \mathbf{u}\cdot\nabla\mathbf{u}) = -\nabla P + \mu\nabla^2\mathbf{u} + \rho\mathbf{f}, \qquad (5.1)$$
$$\nabla\cdot\mathbf{u} = 0.$$

In these equations μ and P are the fluid viscosity and pressure respectively and ρ is the density of both fluid and particles; i.e. neutrally buoyant particles. The coordinate system and velocity components in the simulation are denoted by (x, y, z) and $\mathbf{u} = (u, v, w)$ corresponding to the spanwise, streamwise and wall-normal directions. We use IBM to account for the presence of the finite size particles by applying localised force, $\mathbf{f}$, in the vicinity of each particle surface. The motion of the particles are governed by Newton-Euler equations,

$$m^p\frac{d\mathbf{U}_c^p}{dt} = \mathbf{F}^p, \qquad (5.2)$$
$$I^p\frac{d\mathbf{\Omega}_c^p}{dt} = \mathbf{T}^p,$$

where $\mathbf{U}_c^p$ and $\mathbf{\Omega}_c^p$ are the velocity and rotation rate of particle p, m^p and I^p are the mass and moment inertia and $\mathbf{F}^p$ and $\mathbf{T}^p$ the net force and moment due to the action of hydrodynamic and contant interactions. Those interactions for particles read

$$F^p = \oint_{\partial V_p}[-PI + \mu(\nabla\mathbf{u} + \nabla\mathbf{u}^T)]\cdot\mathbf{n}dS + \mathbf{F}_c, \qquad (5.3)$$
$$T^p = \oint_{\partial V_p}\mathbf{r}\times\big\{[-PI + \mu(\nabla\mathbf{u} + \nabla\mathbf{u}^T)]\cdot\mathbf{n}\big\}dS + \mathbf{T}_c,$$

where ∂V_p represents the surface of the particles with unit normal vector $\mathbf{n}$. The position vector from the centre to the surface of the particle is denoted by $\mathbf{r}$

and the force and torque resulting from particle-particle (particle-wall) contacts are indicated by $\mathbf{F}_c$ and $\mathbf{T}_c$. The no-slip and no-penetration conditions at each point $\mathbf{X}$ on particle surface implies $\mathbf{u}(\mathbf{X}) = \mathbf{U}^p(\mathbf{X}) = \mathbf{U}_c^p + \mathbf{\Omega}_c^p \times \mathbf{r}$. This condition is satisfied indirectly by including IBM forcing, $\mathbf{f}$, on the right hand side of equation 5.1.

5.2. Methods to simulate finite-size particle suspensions

Computer simulations play an important role in developing the theories about the suspensions because, literally everything is known about a simulated system (Campbell 1990). In many applications the goal is to understand the physics of particle-fluid and particle-particle interactions. The challenge here is to employ a numerical method which is able to resolve accurately the flow around individual particles and at the same time is computationally affordable. Obviously the most accurate way is to use an unstructured body fitted mesh everywhere in the domain except the area occupied by particles (see e.g Burton & Eaton 2005; Zeng *et al.* 2009). However, since the particles are moving, regeneration of the mesh is needed at every time step makes the scheme computationally very expensive. The complication increases even more when the particles are of deformable and interact with each other. Employing this method for the dense suspension of thousands of particles is simply impossible. An alternative way is to use a fixed and preferably equispaced mesh grids to solve the flow everywhere even inside the particles. The presence of particles is then treated by applying some kind of force on the grid points inside and/or in the vicinity of the particles. Following this principle, we use Immersed Boundary Method in the scope of the present work. However, first we briefly review some of the other well-known methods.

Force coupling method has been explained and developed in Lomholt & Maxey (2003). In this method the presence of the particles are treated using low order expansion of the force multipoles which is distributed, by a Gaussian function at particle length scale, as body force in the domain. The body force contains monopole and dipole; the monopole incorporates as force, the antisymmetric part of the dipole as torque and the symmetric part as stresslet (Loisel *et al.* 2013). The scheme makes the kinetic energy budget self-consistent as the multiplication of multipole force and particle velocity gives the rate of work by the force in the kinetic energy budget (similar is true for the torque). The main disadvantage of the the method is to not fully resolved the flow very close to the particle surface.

Particles can be modelled in a lattice-Boltzmann solver. In the lattice-Boltzmann (LB) method fluid is modelled by LB points connected through links. The state of the system is integrated in time and space on the LB points by collision rules which guarantees the mass and momentum conservation (Eggels & Somers 1995). Since the operators are local, the implementation and parallelisation of the LB codes are rather easy (Ten-Cate *et al.* 2004). The method can be adopted to simulate the particles in the flow for a broad range

of Reynolds numbers and particle concentrations (Koch & Hill 2001). The nonslip and no penetration boundary conditions on the particle surface are satisfied typically by bounce-back method where the fluid mass propagates through the link which is cut by the particle surface return toward the bulk fluid domain. It is also possible to employ a direct forcing method to satisfy the boundary conditions at the particle surface which is covered by many control points (Ten-Cate *et al.* 2004).

Front tracking method has been derived from the work by Peskin (1977) and developed by Unverdi & Tryggvason (1992), mainly to solve multi-fluid problems where the interface is of finite thickness and deformable. The flow is solved on a set of fixed grid points whereas the interface(front), which is explicitly represented by set of additional gird points, is reconstructed as advected by the flow velocity (see for more details Lu *et al.* 2005, on simulation of bubbles). The flow velocity at the front is obtained from the velocity of the fixed grid points by interpolation. The front is used to update density and viscosity at each grid point and provides a natural way to include the surface tension effect. The major limitations of this method is the difficulties to treat the interfaces that interact and to regenerate the Lagrangian grid points to adjust with the surface stretching or compression.

In Physalis method of Zhang & Prosperetti (2003, 2005), the analytical solution of Stokes flow is used to transfer the nonslip and no penetration condition at the surface of the particle to the neighbouring grids. Using this approximation, the internal boundaries of the suspension can be replaced by known velocities at the fixed grid points. Physalis is a highly accurate method for the suspensions of spherical rigid particles where in addition to hydrodynamic force, torque, stresslet and higher order multipoles of each particle can be captured as a biproduct of the numerical calculations (Sierakowski & Prosperetti 2015). However, the model presented in Zhang & Prosperetti (2005) cannot be applied for deformable and non-spherical particulate flows because there is no analytical solution of Stokes flow for those cases. One of the main advantageous of this method is that the computational cost for a fixed domain size is almost independent of the number of particles which makes the method attractive for simulating denser suspensions.

Last but not the least the Immersed Boundary Method is recently used more often to simulate the particulate flows of finite size particles. In the present work we use IBM with the direct forcing developed by Uhlmann (2005) and modified by Breugem (2012). The details about the method and the numerical treatments are given in the following section.

5.3. Immersed Boundary Method

In the present work we simulate the particles in the flow using Immersed Boundary Method. According to the definition by Mittal & Iaccarino (2005), IBM is generally regarded as a method to solve viscous flow with immersed boundaries, on grids which are not necessarily conform the shape of those boundaries.

Therefore incorporating the boundary conditions requires modification in the governing equation in the vicinity of those boundaries. As mentioned, the challenge here is to provide sufficient accuracy close to the boundaries which should be imposed indirectly using a great number of the background grid points. The main gain is to avoid the complication to conform the mesh around the particles at every time step. IBM suggests a fixed and often uniform structured grid for the fluid phase which makes it easy to be manipulated and at the same time is computationally efficient (Breugem 2012). Based on the argument in Mittal & Iaccarino (2005), the general approach to treat the boundaries in IBM is to add a source (forcing term) in the equations. This can be done by either two general ways: 1) Continues forcing approach where the IBM force is applied on right hand side of the Navier-Sokes equation and then the equation is discretised 2) Discrete forcing approach where N-S equation is first discretised and then the discretisation is adjusted close to the boundaries to account for the presence of the particles. The IBM used in the particle suspension belongs to the first category however the CPL code employed by Giannetti & Luchini (2007) and its modified version in Lashgari *et al.* (2012); Haque *et al.* (2012) are of the second approach. In the CPL code direct boundary condition imposition of the discrete forcing approach is employed by means of ghost cells in the solid and at the vicinity of the fluid.

In the IBM employed in our simulations of particulate flows two set of grid points are considered; fixed Eulerian mesh everywhere in the domain where the fluid is solved and Lagrangian mesh representing the surface of each particle. A regularised delta function is used to communicate between the two grids via interpolating the velocity and spreading the force over three adjacent Eulerian grid points. This makes the interface smooth and effectively similar to a porous surface which avoids high frequency oscillations of force and torque on the particles and provides 2^{nd} order accuracy in the velocity interpolation only if considering the effective particle diameter. In the interpolation and spreading, the force and torque that fluid and particle exert on each other should be preserved. Therefore, the distribution of both Eulerian and Lagrangian grid points are set equispaced with similar spacing. The Crank-Nikelson scheme is used for the viscous term while the nonlinear term is treated explicitly using three-step Runge-Kutta scheme. The spatial derivatives are obtained by second order central difference scheme. The translational and rotational velocity of the particle is updated using the Newton-Euler equation discretised by Runge-Kutta scheme. The IBM force is computed in three steps: 1) Interpolate Eulerian velocity field on the Lagrangian grid points 2) Calculate the IBM force on the Lagrangian grid points based on the difference between the interpolated velocity and particle velocity at those points 3) Spread the IBM force from Lagrangian to the Eulerian grid points. The IBM force is calculated based on the first correction velocity. Once the force is spread from Lagrangian to Eulerian grids, it contributes to update the second correction velocity. The pressure correction is then applied by solving for the second correction velocity

which enforce the continuity condition and update the velocity for the next time step (Breugem 2010).

Once a particle approaches another particle or the wall, the squeezed flow between the two solid objects induces force known as lubrication force. The normal component of the lubrication force varies as $1/\epsilon$ and the tangential component as $log(\epsilon)$, where ϵ is the normalised gap width. Simulating two spheres in a squeezing motion shows that for the normal component of lubrication force a resolution-dependent lubrication correction is needed to capture the dynamics between the spheres (see Lambert *et al.* 2013); the IBM force underestimates the lubrication force. The lubrication correction, based on asymptotic analytical solution of Brenner (1961) is included when the gap distance between two approaching particles becomes much smaller than the grid spacing (Breugem 2010). For the tangential component however, the simulation of a particle pair in shearing motion shows that the lubrication correction is not needed even at $\epsilon \to 0$ where zero relative velocity at the point of contact provides finite tangential force.

The asymptotic expansion for the lubrication correction force is diverged at $\epsilon \to 0$ where in reality the surface roughness effect avoids the infinity force. The surface roughnesses affect the dynamic of the near field interactions. As an example Cunha & Hinch (1996) show that in the absence of inertia the intercation between two spheres can be irreversible depending on their surface roughness. In the code, the effect of the roughness is captured by fixing the lubrication force at very small gaps before the collision takes place. Once the collision occurs the lubrication correction is turned off and soft sphere collision force becomes active.

The soft sphere model allows overlap between the particles. The normal force is calculated as a function of the overlap and the relative normal velocity of the particles. The coefficient of restitution, e, is defined by the ratio between the relative velocity of the particles before and after the collision. The duration of the collision is given by a multiplication of $N_c = 8$ and the time step, Δt. The coefficient of the soft collision force is then directly obtained based on the coefficient of restitution and the collision time. The collision time cannot be too long to avoid extreme overlapping and not too short to avoid restriction on the numerical time step (Breugem 2010).

CHAPTER 6

Transition and turbulence

In the present work we simulate the suspension of finite size particles in channel over the range of bulk Reynolds number, $500 \leq Re \leq 5000$. Typically in unladen channel or pipe flow we observe laminar, turbulent and transitional regimes in this range of the Reynolds numbers. Therefore, here we review some studies on the transition and turbulent particulate flows in a channel or pipe.

6.1. Transition in particulate flows

Many years after the seminal work by Reynolds (1983) research on flow transition from laminar to turbulent regime is still a hot topic in fluid mechanic. The primitive and the most important reason for the vast amount of studies is the large difference between the behaviour of laminar and turbulent flows. In particular, the force needs to derive the flow increases significantly when the turbulent regime emerges. Despite the complexity in understanding different mechanisms in the transition of Newtonian fluids, parallel investigations have also been conducted on the transition of complex flows. Here we review some studies on transitional particle laden flows.

The subcritical transition to turbulence in the presence of small particles is studied by Klinkenberg *et al.* (2013) using a two way coupling model. They found that the particles at low number density facilitate the transition. Opposite is true at higher concentrations when more energy is needed to bring the system to turbulence. Results show that heavy particles may not influence the optimal growth based on the linear theory because particle relaxation time is much shorter than the transient time of the growth of the streamwise elongated structures, streaks. However, particles contribute to the secondary instability and streak breakdown.

Considering the transition in finite size particulate channel flow, Matas *et al.* (2003) conduct a set of experiments on suspension of neutrally buoyant particles in a pipe. They provide the critical threshold of the subcritical transition form laminar to intermittent regime, where turbulent spot start to grow, as a function of particle concentration and the ratio between pipe to particle diameter, D/d. The spectra of the pressure drop between the entrance and exit of the pipe is used to determine the flow regime. For small particles where the ratio $D/d \geq 65$ they find a monotonic increase in the critical threshold. The delay in the transition is attributed to the enhancement in of the effective

viscosity of the suspension in the presence of rigid particles. On the contrary, when particles are large, $D/d < 65$, flow exhibits a non-monotonic behaviour of the critical threshold. The critical Reynolds number first decreases and then increases as the volume fraction increases. The strongest non-monotonic behaviour is observed for the case of $D/d \approx 10$. This motivates our choice of particle size in the current study. The promotion of the transition is attributed to the disturbances induce by large enough particles which are less efficiently damped by the action of viscous dissipation. Scaling the data of the small particles by the effective viscosity, a new critical Reynolds number, independent of Φ, is obtained. However, at very high concentration $\Phi > 0.25$, this new critical Reynolds number increases sharply suggesting the presence of an additional dissipation mechanism. Later on Yu *et al.* (2013) perform numerical simulation aiming to reproduce the results of the experiment by Matas *et al.* (2003). Since particles disturb the flow at all the Reynolds numbers, they compute the maximum streamwise velocity fluctuation energy, E, of the mixture and denote the flow laminar or turbulence if E is larger or smaller than a certain threshold, E_c. The results then depend on the choice of E_c.

The effects of the finite size particles in the flow transition and critical threshold can be divided into two parts. First the balance between the disturbance and dissipation induce by the particles. The disturbances (agitations) in the particle suspensions may come from the random velocities of the particles due to hydrodynamic and inter-particle interactions. The driving force for both mechanisms is the velocity gradient as mentioned in Campbell (1990). The strength of those agitations depends on the particle size. In Lashgari *et al.* (2015) we show that the initial wall normal position of the particles changes the level of disturbances induced by the particle due to the nonuniform background shear and this affects the flow transition fixing the other parameters of the simulation. Once the flow becomes turbulent, it sustains at the lower Reynolds number than the one of the unladen flow. Large particles produce strong disturbances that cannot be damped completely by the viscose dissipation.

The second effect is the interactions between the particles and the flow coherent structures. Loisel *et al.* (2013) show that for a fixed volume fraction of 5%, turbulent flow sustains in the channel at lower Reynolds number than that of the unladen flow. They relate the reduction of the critical threshold to the break down of the coherent structure by particles into many small and more energetic structures. The effect of finite size particles at the initial stage of the transition and lift-up mechanism are examined in Brandt (2014). Lift-up mechanism, the formation and growth of the streamwise velocity perturbation by cross flow disturbances, known as a key process to promote subcritical transition and sustained turbulence in shear flows. The simulations of Couette flow suspended with finite size particles at low volume fraction shows that the streaks formation and growth are not modified significantly and particles mainly contribute to induce the secondary stability on the streaks and promote

transition. Similar behaviour is also observed in Lashgari *et al.* (2015) in the channel flow suspended by few finite size particles.

6.2. Turbulence in particulate flows

Turbulent flow of suspension is one of the most complicated systems in fluid mechanics because both turbulence and multiphase flow are not well-understood and the combination pose a formidable challenge (Balachandar & Eaton 2010). Campbell in his annual review (Campbell 1990) states that "*Obviously, a theory for the flow of particles within an interstitial fluid that considers in full the interaction between the particles and the turbulence of the fluid is too complex to be handled exactly.*" Despite complexity, studying the turbulent flow of suspension is essential not only form fundamental perspective but also due to the practical reasons, i.e. turbulence is necessary to maintain the slurry suspended and well-mixed (Ten-Cate *et al.* 2004).

In many studies turbulent particulate flow is considered at dilute or semi-dilute regime where one-way or two-way coupling approach is employed (see Annu Rev by Balachandar & Eaton 2010). The dynamics of dispersed phase are examined extensively focusing on particle transport, spatial concentration and diffusion (see e. g. Squires & Eaton 1991). In unbounded flows it is shown that the heavy particles form a fracture structures (Bec *et al.* 2007) whereas in wall bounded flows turbophoresis, particle accommodation close the the wall, is observed and its strength is connected to the ratio between particle and fluid time scales (Reek 1983; Soldati & Marchioli 2009).

Considering the effect of particles on the fluid phase, turbulence modulation is also studied extensively (Squires & Eaton 1990; Li *et al.* 2001; Ferrante & Elghobashi 2003; Zhao *et al.* 2010). As reported in Balachandar & Eaton (2010) turbulence modulation mechanisms are 1) additional dissipation due to the presence of the particles, 2) transfer the energy form fluid to particle and 3) creation of vortex shedding behind the particles. Gore & Crowe (1989) show that the critical parameter to indicate whether the turbulent activity is suppressed or enhanced is the ratio between the particle diameters and the relevant length scale in the fluid phase. Small particles absorb the energy of the eddies via drag force reducing the turbulence intensity. The large particles however tend to create disturbances and contribute to the enhancement of the turbulent intensity.

In many high Reynolds number suspension flows the typical particle size is much larger than the Kolmogorov length scale and particles and fluid are fully interact. However, few studies consider the turbulent flow of finite size particles where the flow is resolved around each particle. Ten-Cate *et al.* (2004) report the influence of finite size particles on the spectrum of a isotropic turbulent flow. They observe that the kinetic energy decreases at large scales and energy dissipation increases at the wavenumbers close to the particle size; particle generates flow motion and enhance dissipation. Similar behaviour is observed

in the experiment by Bellani *et al.* (2012) on both spherical and ellipsoid particles in the isotropic turbulent flow. However, they show that the ellipsoids remove relatively less turbulent kinetic energy at large scales with respect to the spheres.

In the near wall region of an open channel flow, finite size heavy particles tend to reside in low speed streaks and therefore the mean particle velocity is lower than the one of the fluid velocity (Kidanemariam *et al.* 2013). Considering the turbulent channel flow of finite size particle suspension, Picano *et al.* (2015) show that the mean flow profile in the log region, $U^+ = \frac{1}{\kappa} lny^+ + B$ where κ is the *Kármán* constant and B is the additive coefficient (Pope 2000), changes considerably in the presence of the particles. The *Kármán* constant reduces which suggests turbulent drag reduction similar to the polymeric turbulent flow while the additive constant also decreases indicating the drag enhancement. The latter effect is shown stronger so that the net result is still an increase in the overall drag. Particles alter the near wall structures significantly. The spacing in the near wall streak increases while the contrast between the high and low velocity is weakened.

Even though by increasing the Reynolds number fluid flow often experiences a transition from laminar to turbulent regime, as we will show in this work, it is not always possible to identify the transition threshold of the particulate flows by monitoring different observables such as the level of the flow fluctuations, especially when the volume fraction of the solid phase is large (smooth transition). We need to employ a quantitative measure to identify the characteristics of the different regimes of the inertial suspensions.

CHAPTER 7

Bulk behaviour of inertial suspensions

In this chapter we focus on the bulk behaviour of the inertial suspensions. In particular we discuss the suspension stress, effective viscosity, shear-thickening and the analogy to the seminal work by Bagnold (1954).

7.1. Suspension stress

Stress in multiphase flows is one of the most complicated issues which has been subjected to many studies, among others Batchelor (1970); Marchioro *et al.* (1999); Prosperetti (2004). In continuum-mechanical approach suspension is considered as a continuum mixture consists of two interacting phases. To study the stress in the suspensions, a specification of stress for each phase plus a relation for the interactions between the phases are needed. To tackle this problem, some sort of averaging process is required to connect the macroscopic behaviour of the suspension to those of the microscopic structures (Drew 1983). However, opposite to some average quantities like particle mean velocity where its corresponding counterpart at microscopic level is tangible, the quantity like mixture stress is meaningful only at macroscopic level (Marchioro *et al.* 2000).

Batchelor is probably the first to derive the relation for the stress in the particle suspension (Batchelor 1970). The main assumption in his derivation is that in the region away from the wall the volume averaged of a certain quantity like stress over a big enough volume is equal to the local ensemble average. Therefore, the averaging is done on a volume of many particles where the local variation of the quantity is negligible; the statistical local homogeneity condition as denoted in Jeffrey & Acrivos (1976). In other words the volume averaging of Batchelor is valid if particles are much smaller than the macro-scale (Prosperetti 2008). The averaged stress equation is also derived in Zhang & Prosperetti (1994) where opposite to Batchelor, the authors use ensemble averaging which allows the problem formulation even at spatial non-uniformity.

Following Zhang & Prosperetti (1994); Marchioro *et al.* (1999); Zhang & Prosperetti (2010), the force balance equation for the two phase flow on the volume $\mathcal{V}$ with boundary $\mathcal{S}(V)$ reads

$$\rho \int_{\mathcal{V}} (\xi \boldsymbol{a}^p + (1-\xi)\boldsymbol{a}^f)\, d\mathcal{V} = \oint_{\mathcal{S}(V)} [\xi \boldsymbol{\sigma}^p + (1-\xi)\boldsymbol{\sigma}^f] \cdot n\, dS. \tag{7.1}$$

In this expression ξ is the phase indicator with values $\xi = 0$ for the fluid and $\xi = 1$ for the particle phase. We denote the stress and acceleration of

the fluid and particle phase by $\boldsymbol{\sigma}^f$, $\boldsymbol{a}^f$, $\boldsymbol{\sigma}^p$ and $\boldsymbol{a}^p$ respectively. Assuming statistical homogeneity in the streamwise and spanwise directions, one can obtain an expression for the stress budget across the channel, (for the details of the derivations see the Appendix of Picano *et al.* 2015),

$$\frac{\tau(z/h)}{\rho} = -\langle v'^t w'^t \rangle + \nu(1-\varphi)\frac{dV^f}{dz} + \frac{\varphi}{\rho}\langle \sigma^p_{yz} \rangle = \nu \frac{dV^f}{dz}\bigg|_w (1-\frac{z}{h}), \qquad (7.2)$$

where V^f is the mean streamwise fluid velocity and $\tau(z/h)$ is the total stress as a function of wall normal coordinate, z, normalised by the channel half width, h. The first term in the stress budget is the total Reynolds stress, $\frac{\tau_R}{\rho} = \langle v'^t w'^t \rangle = (1-\varphi)\langle v'^f w'^f \rangle + \varphi \langle v'^p w'^p \rangle$, consisting of the fluid and particle Reynolds stress weighted by local particle volume fraction, φ. The fluid Reynolds stress is defined when an element of the fluid exchange its momentum with the host fluid and this is derived by the gradient of the fluid velocity (shear). Opposite is true for the particle Reynolds stress where the transfer of the particles is not governed by the gradient of the particle velocity (Elghobashi 1994). Particle Reynolds stress is indicated as streaming mode in Campbell (1990) where the particles carrying the momentum by their own motion. The second term, $\frac{\tau_V}{\rho} = \nu(1-\varphi)\frac{dV^f}{dz}$, is the classical viscous stress resulting form the action of the carrier fluid viscosity. The last term, $\frac{\tau_P}{\rho} = \frac{\varphi}{\rho}\langle \sigma^p_{yz} \rangle$, is the stress due to the particles which is described in more details in the following. The sum of the three terms is a linear function across the channel, as for the classic turbulent flow (Pope 2000), with the wall shear stress, $\frac{\tau_w}{\rho} = \nu \frac{dV^f}{dz}\big|_w$. Here we show in figure 7.1 as an example the stress budget for a channel flow of neutrally buoyant particles at bulk $Re = 2000$ and $\Phi = 0.1$ where the particle diameter is fixed to $d = 2h/10$. Similar to the turbulent unladen flow, we observe that the viscous stress is strong at the wall and Reynolds stress is large between the wall and core region. However, an additional contribution of particle stress is also evident especially close to the wall. In general all the three contributions exist in the budget of the particle suspension with different relevance depending on the Reynolds number and particle concentration.

The expression for the particle stress is discussed in details in Batchelor (1970); Kulkarni & Morris (2008); Zhang & Prosperetti (2010). Following Batchelor (1970), the particle stress in the absence of an external torque reads

$$\sigma^p_{ij} = \frac{1}{V}\Sigma_V \int_{A_p} \frac{1}{2}\{\sigma_{ik}x_j + \sigma_{jk}x_i\}n_k dA - \frac{1}{V}\Sigma_V \int_{V_p} \frac{1}{2}\rho\{f'_i x_j + f'_j x_i\}dV + \sigma^c_{ij}, \qquad (7.3)$$

where f'_i is the local acceleration of the particle relative to the average value of the acceleration in volume V, x is the material point, A_p and V_p are the particle surface area and volume and $\sigma_{ij} = -P\delta_{ij} + \mu(\frac{\partial \mathbf{u}_i}{\partial x_j} + \frac{\partial \mathbf{u}_j}{\partial x_i})$ is the fluid stress tensor. Note that in the Batchelor formulation the higher order moments are neglected because of the assumption of uniform stress state (see Nott *et al.* 2011, for more details). The first term on the right hand side of equation 7.3

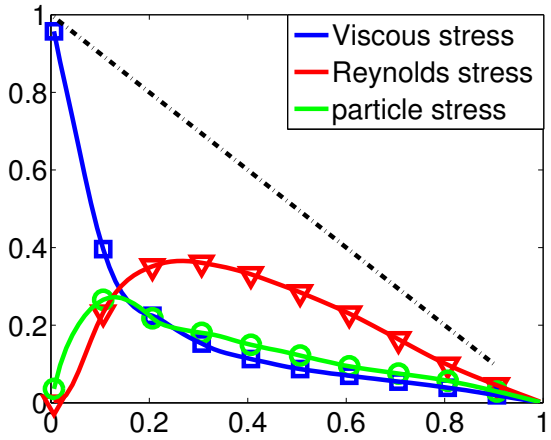

FIGURE 7.1. Stress budget for $Re = 2000$, $\Phi = 0.1$ & $2h/d = 10$

is the hydrodynamic stresslet resulting from the symmetric and traceless part of the shear stress. This is related to effective viscosity in dilute suspension (Prosperetti 2004). The second term is related to stress inside the particle assuming the absence of all non-hydrodyamic forces and is obtained by considering particle acceleration and rotation with respect to the neighbouring flow (see Nott *et al.* 2011; Haddadi & Morris 2014). The interpretation and meaning of the pressure and stress inside the rigid particle is not clear as denoted in Marchioro *et al.* (1999), however it emerges in the average equation of the two phase flow. The last term is the inter-particle stress which originates from the near-field particle interactions. Including inertia in the suspension new and effective ways to transport the momentum by the particle phase emerges such as particle Reynolds number and particle acceleration (Kulkarni & Morris 2008).

In Lashgari *et al.* (2014), stress budget analysis is employed to identify different inertial regimes in the suspension of neutrally buoyant finite size rigid particles. The simulations are performed at fixed particle diameter, $d = 2h/10$, varying the particle concentration and Reynolds number. For each case, the stress budget is obtained (like figure 7.1) and the contribution of each stress term is averaged across the channel. Following this procedure the phase diagram of the stress budget is created as shown in figure 7.2 . In the phase diagram different colours represent the region where the contribution of each stress term is the largest. The solid black lines show the boundary of the regions where the contribution of each term is more than 50% of the total stress. These regions represent laminar, turbulent and inertial shear-thickening regimes where the contribution of viscous, Reynolds and particle stress is the largest (relative majority). All three regimes are coexist with different relevance depending on the Reynolds number and particle volume fraction. The inertial shear thickening

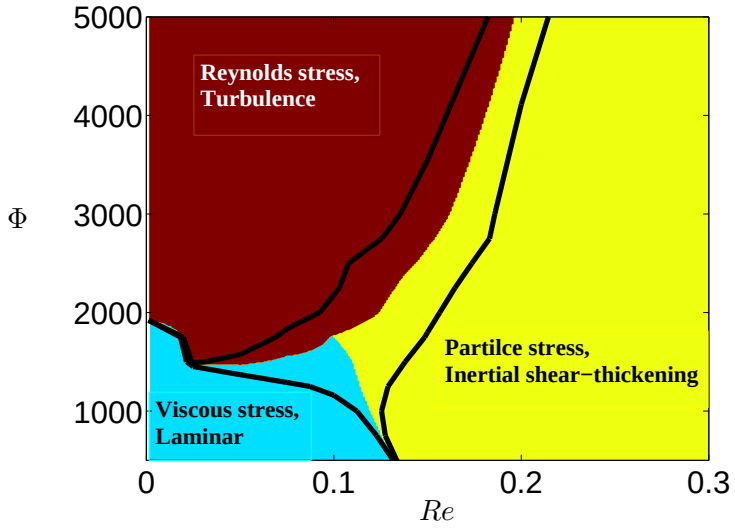

FIGURE 7.2. Phase diagram of stress budget for the simulation of the particles $2h/d = 10$, figure is taken form Lashgari *et al.* (2014)

regime is defined as a regime when we observe a significant enhancement in the effective viscosity (normalised wall shear stress) of the suspension and this is not attributed to the Reynolds stress but particle stress.

7.2. Effective viscosity and shear-thickening

Effective viscosity is an important quantity to study due to its direct connection to the energy consumption when deriving the suspension through configurations like pipe and channel. Adding even few particles in a Newtonian fluid, the mixture viscosity differs from the one of the unladen flow. The first theoretical approach to understand the rheology of the suspension has been introduced by Einstein (1906) where he proposed a formula for the effective viscosity of the suspension to the first order of the particle concentration, $\mu_{sus}/\mu_{liq} = \mu_r = 1 + 2.5\Phi$, in the absence of inertia. The Einstein's formula is obtained by assuming each particle contributes individually to the total dissipation; i.e. dilute regime (Jeffrey & Acrivos 1976). Batchelor & Green (1972) expand the formula to the second order of the particle concentration accounting partially the mutual interactions between the particles. For higher concentrations several empirical fits to the experimental data are introduced, among other Eilers fit (Stickel & Powell 2005) where the effective viscosity reads, $\mu_r = (1 + B\frac{\Phi}{1-\Phi/\Phi_{max}})^2$. In the expression $B = 1.25 - 1.5$ and Φ_{max} is the maximum packing fraction and is chosen 0.58 for the glass transition or 0.64 for random close packing (Shewan & Stokes 2015). Note that generally Φ_{max} depends on the shear rate, particle size and shape (Konijn *et al.* 2014).

Not only the mixture viscosity itself but its variation under the applied shear is important. In many cases suspensions exhibit shear-thickening in the presence of inertia. Shear-thickening is one of the common aspects of the non-Newtonian fluids which is defined by an increment in the viscosity of the mixture as subjected to shear (Bird *et al.* 1987). From the fundamental science prospective, shear-thickening is an intriguing phenomenon occurs by simply adding few rigid spheres in a Newtonian fluid (Brown & Jaeger 2014). The origin of shear-thickening in the suspensions has been widely investigated. Yeo & Maxey (2013) relate shear-thickening to the induced normal lubrication interactions near the compressive principal axis of shear flow. Hydro-clustering of the particles by lubrication force, disordering the particle layers from structured to unstructured and dilatancy as an increase in the volume of particulate packing are the three major mechanisms for shear-thickening (Brown & Jaeger 2014). In the work by Picano *et al.* (2013) shear-thickening in the presence of non-negligible inertia is attributed to an additional excluded volume, i.e., the shadow region behind each particle where it is unlikely to find a second particle.

Finally we note that the inertial shear-thickening is distinct from Discontinues Shear-Thickening. In the latter, as the particle volume fraction increases, the dynamics of the suspension changes toward a jamming state and DST may occurs where stress exhibits a jump as shear-rate increases (Brown & Jaeger 2012). Opposite to DST, here we are dealing with the inertial shear-thickening which occurs at lower volume fractions and higher shear rates. In the inertia shear-thickening regime we observe an enhanced contribution of the particle phase in the total stress as Re increases.

7.3. Bagnoldian dynamics

The seminal work by Bagnold (1954) can be assumed as a pioneer study of the suspension of neutrally buoyant particles. Performing a set of experiments on a suspension between two concentric drums, Bagnold intuitively understood that shearing grains in viscous fluid results in dispersive pressure (radial stress) in additional to the shear stress. At low shear rate the regime is viscosity dominated and the wall shear stress can be estimated by the fluid viscosity modified due to the presence of the grains. In this macro-viscous regime a linear function describes the relation between shear and dispersive stresses to the shear rate. Different behaviour is observed at high shear rate where inertia dominates the dynamics and the contribution of grain stress is added to the fluid stress. In the grain inertia regime both shear stress and dispersive pressure become proportional to the square of shear rate. The quadratic variation of the shear stress by shear rate, inertial effects, resembles the dynamics of the dry granular material which are known as the limiting case of the dense suspension when the effect of interstitial fluid is negligible (Campbell 1990). Different regimes in the suspensions are defined by the Bagnold number, $Ba = 4Re_p\sqrt{\lambda}$, where $\lambda = \frac{1}{(0.74/\Phi)^{1/3}-1}$ is the linear concentration represents the ratio between the particle dimeter to the average spacing between the particles. Bagnold

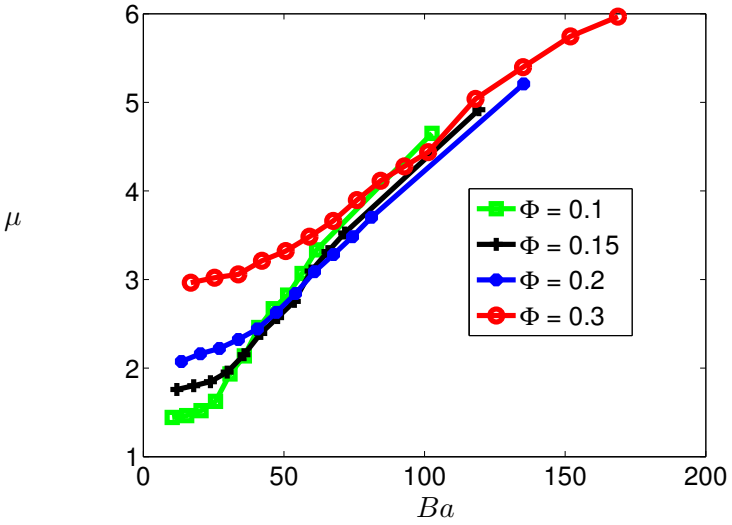

FIGURE 7.3. Effective viscosity versus Bagnold number for the simulation of the particles $2h/d = 10$, figure is taken form Lashgari *et al.* (2016)

number shows the ratio between the inertia to viscous stress. This ratio is small, $Ba \leq 40$, for the micro-viscous regime and large, $Ba \geq 450$, for the grain-inertial regime. Bagnold predicts that by increasing the concentration of the solid phase the fluid shear stress due to the turbulent fluctuations progressively gives place to the grain stress.

Not much is done after the work by Bagnold to measure or compute quantitatively the properties of the different regimes. Fall *et al.* (2010) employ similar experimental setup and report that the local rheology exhibits a continuous transition at low shear rate from viscous to Bagnoldian regime and the shear stress of the transition does not depend on the particle volume fraction. In figure 7.3 we show the effective viscosity pertaining our simulations in Lashgari *et al.* (2016) versus the Bagnold number for four representative values of the particle volume fraction. Interestingly, we observe that the effective viscosity of the suspension is almost constant when $Ba < 40$, as expected in the macro-viscous regime where the shear stress depends linearly on the shear rate. When $Ba > 70$, all the curves collapse on a single line and the effective viscosity varies almost linearly with the Bagnold number. This suggests that the Reynolds stress and particle dominated regimes may share similar Bagnold number while their underlying physical mechanisms are different.

CHAPTER 8

Particle dynamics in inertial suspensions

In this chapter we examine the particle dynamics in inertial suspensions. In particular, we discuss the particle distribution, dispersion and collision dynamics.

8.1. Particle migration, concentration profile

The spatial structure of the particles is the key to make the complexities in the behaviour of particle suspensions (Butler 2014). Particle preferential concentration in the flow is an interesting topic because it is related to many applications such as droplet formation, particle settling, turbulent modulation and wall shear stress (Eaton & Fessler 1994). Particle concentration in homogenous isotropic turbulence is widely studied from dissipative to inertial scales; (see as examples Eaton & Fessler 1994; Bec *et al.* 2007). The general agreement here is that the particles of high inertia tend to accommodate in the region of high strain however those of low inertia are trapped in the region of high vorticity (see as an example Sundaram & Collins 1997). In wall bounded flows several mechanisms such as turbophoresis, shear-induced migration, Segre-Silberberg effect and turbulent mixing are known to contribute to the arrangement of the particles in the domain (Uhlmann 2008). Turbophoresis is attributed to the migration of the particles in the direction of turbulent intensity gradient where a global maxima in the profile of the local particle volume fraction is observed at the wall (Caporaloni *et al.* 1975). Here we discuss the other three mechanisms in connection with the flow cases from different inertial regimes introduced above.

We show in figure 8.1 the profile of the local volume fraction, $\phi(z)$, of the three cases corresponding to the different inertial regimes. For each case the profile is normalised by its bulk particle concentration denoted as Φ_m. At $Re = 500$ and $\Phi = 0.05$, the flow regime is laminar (see figure 7.2). We observe that the wall and core of the channel is almost empty from the presence of the particles and they tend to accommodate in some preferential equilibrium positions across the channel due to the Segre-Silberberg effect (Segré & Silberberg 1961). The interaction between the particle stresslet and the curvature in background velocity profile induces a lateral force toward the wall (Saffman 1965; Matas *et al.* 2004; Abbas *et al.* 2014). The balance between the lateral force and the wall-flow interaction provides the equilibrium position of an inertial particle in a channel (Eckstein *et al.* 1977; Chun & Ladd 2006).

At high Reynolds numbers and yet moderate values of the particle volume fraction, i.e $Re = 5000$ and $\Phi = 0.05$, the flow regime is turbulent and we observe that the distribution of the particles is homogenised across the channel (except close to the wall due to the one-sided interaction) under the action of the turbulent eddies. The effect of the turbulent mixing on the particle concentration is mainly studied for point particles in homogeneous isotropic turbulence where particle concentration depends on the Stokes number and the separation between the particles and fluid length scale (Eaton & Fessler 1994; Bec *et al.* 2007).

At large volume fraction, we observe a significant accommodation of the particles in the core of the channel due to the shear-induced migration as shown in figure for $Re = 2500$ and $\Phi = 0.3$. Similar behaviour is observed in other configurations; i.e. in annular Couette flow (Abbott *et al.* 1991; Dbouk *et al.* 2013), in duct flow (Chun & Ladd 2006; Abbas *et al.* 2014), in a cylindrical conduit (Hampton *et al.* 1997) and vertical gas turbulent channel flow (Li *et al.* 2001). Shear-induced migration occurs from the region of high to low shear rate even in the absence of inertia and particle surface roughness (Guazzelli & Morris 2011; Leighton & Acrivos 1987). It is attributed to the imbalance in the pressure across the channel; i.e. divergence of the particle stress (Nott & Brady 1994; Dbouk *et al.* 2013). Shear-induced migration is not limited to the spherical particles and also observed in the suspension of rod-like particles between an annular rotating cylinder (Mondy *et al.* 1994). The accommodation of the particles in the core of the channel blunts the mean velocity profile and reduces the correlation between the streamwise and wall normal fluid velocities as shown in Uhlmann (2008). In the core region momentum is transported by the plug flow of the particles as in the granular medium and the hydrodynamic interactions are less effective. We also observe a layering of the particles at the wall due to the action of vortices which push the particles into the viscous layer where they are trapped (Eaton & Fessler 1994). The accommodation of the particles close to the wall brings the momentum toward the wall and contributes to the enhancement of the wall friction.

In conclusion we show that different mechanisms drive the migration of the particles at low and high particle volume fractions as denoted by Hampton *et al.* (1997).

8.2. Particle dispersion

Particle dispersion is related to the mixing and transport of the solid material through the suspensions. This is a relevant quantity in many applications such as pulp handling, fluidised bed and cement transport (Cunha & Hinch 1996; Breedveld *et al.* 1998). From the biological point of view, dispersion of the particles is also important in extracorporeal devices, formation of the clot and oxygen transport with red blood cells (Eckstein *et al.* 1977). For more discussions in this topic we encourage the readers to see Breedveld *et al.* (1998);

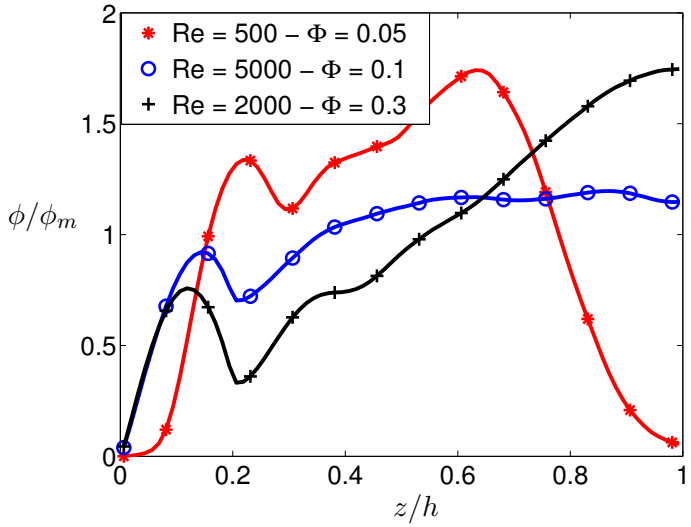

FIGURE 8.1. Profile of normalised local volume fraction as a function of wall normal coordinate for the cases indicated in the inset.

Eckstein *et al.* (1977) as well as Abbas *et al.* (2009) for the theoretical modelling based on kinetic theory of the granular media.

Considering stokes flow, two spheres passing each other in a simple shear flow return to their original streamline and no dispersion happens. However, if the number of particles increases, the symmetry of the Stokes flow breaks (irreversibility) and dispersion takes place (Leighton & Acrivos 1987; Koh *et al.* 1994). Including inertia, even the trajectory of two particles exhibit lateral displacement as shown among others by Eckstein *et al.* (1977); Kulkarni & Morris (2008). The hydrodynamic and inter-particle interactions in suspension induce irregular motion and lateral migration of the particles from their instantaneous average trajectories. This is different than shear-induced gradient diffusivity where non-uniformity of the particle concentration is the driving mechanism for the dispersion (Breedveld *et al.* 1998).

The mean square displacement of the particles is used to measure the particle dispersion and is defined by,

$$\langle \Delta x_p^2(\Delta t) \rangle \quad = \quad \langle [x_p(t+\Delta t) - x_p(t)]^2 \rangle_{p,t}, \tag{8.1}$$

for the spanwise component, where $x_p(t)$ is the spanwise trajectory of the particle p. Similar formula applies for the other components. At small Δt, the particle trajectories are correlated and $\langle \Delta x_p^2 \rangle \propto (\Delta t)^2$. At large Δt, the mean square displacement becomes a linear function of Δt indicating the de-correlation of the particle trajectories. The half of the slope of the linear part of mean square

displacement gives the dispersion coefficient, $D_{xx} = \langle \Delta x_p^2(\Delta t) \rangle / 2\Delta t$. Dispersion coefficient is generally proportional to the shear rate and the square of the particle radius (Breedveld *et al.* 1998). We observe in Lashgari *et al.* (2016) that particle dispersion is generally lower for the inertial shear-thickening than for the turbulent cases. At high particle concentrations the lateral migration of the particles is low in average due to the significant particles accommodation in the channel centre whereas turbulent mixing induces chaotic particle motion.

8.3. Pair-particle relative velocity and collision

The dynamic of the collisions in a suspension has beed studied to model many natural and industrial processes like formation of raindrop and pneumatic transport. In this context the advantages of the numerical simulation becomes more evident because the details of the particle trajectories and pair-particle interactions can be stored and analyse over a long period.

The main ingredients of the collision dynamics are a measure of pair-particle relative position and velocity. The former is usually studied by computing pair distribution function, $G(r, \theta, \psi)$, of finding a particle respect to second particle at distance r from the centres and polar and azimuthal angles, θ and ψ. The knowledge about G can be directly connected to the bulk behaviour of the suspension. As an example, Yeo & Maxey (2013) show that the effective viscosity of the suspension is attributed to the increase in the probability of the events near the compressive principal axis. In this work we use polar and azimuthal averaged probability distribution function, known as Radial Distribution Function, $g(r)$. Radial distribution function is used to determine the level of anisotropy in the suspension (Kulkarni & Morris 2008). RDF is the averaged number of particle centres located in a shell of radius r and $r + dr$ divided by the expected number of particles of a uniform distribution (see Reade & Collins 2000; Gualtieri *et al.* 2009). It is defined by

$$g(r) = \frac{1}{4\pi} \frac{dN_r}{dr} \frac{1}{r^2 n_0}, \tag{8.2}$$

where $n_0 = 0.5 * N_p(N_p - 1)/V$ is the density of particle pairs in the volume V, with N_p the total number of particles and N_r is the number of particle pairs in a sphere of radius r. For small values of r, $g(r)$ shows the intensity of the particle clustering whereas $g(r) \to 1$ when $r \to \infty$ indicating uniform distribution.

Collision is also driven by relative velocity between the particles which in turn is affected by the flow fluctuations around the pair-particles (Gualtieri *et al.* 2012). The normal relative velocity of particle i and j is obtained by

$$\Delta v_n(r_{ij}) = (\mathbf{u}_i - \mathbf{u}_j) \cdot \frac{(\mathbf{r}_i - \mathbf{r}_j)}{|(\mathbf{r}_i - \mathbf{r}_j)|} = (\mathbf{u}_i - \mathbf{u}_j) \cdot \frac{\mathbf{r}_{ij}}{|\mathbf{r}_{ij}|}. \tag{8.3}$$

The normal relative velocity is a scalar quantity and can be either positive, $\Delta v_n^+(r_{ij}) = \Delta v_n(r_{ij})\big|_{>0}$, for departing particles or negative, $\Delta v_n^-(r_{ij}) = \Delta v_n(r_{ij})\big|_{<0}$, for approaching particles. Therefore the averaged normal relative velocity can be decomposed into $\langle \Delta v_n(r) \rangle = \langle \Delta v_n^+(r) \rangle + \langle \Delta v_n^-(r) \rangle$. The relative motion of the particles approaching each other, $\langle \Delta v_n^-(r) \rangle$, tends to vanish as they get very close to each other where the lubrication force dominates the dynamic (Brady & Bossis 1988). Similar behaviour is observed for $\langle \Delta v_n^+(r) \rangle$ because lubrication force is attractive when particles separate (Ten-Cate *et al.* 2004). As r increases the magnitude of $\langle \Delta v_n^-(r) \rangle$ increases monotonically indicating that pair-particles are less strongly correlated (Sundaram & Collins 1997).

Finally, the collision kernel is obtained by multiplication of $g(r)$ and $\langle \Delta v_n^-(r) \rangle$,

$$\kappa(r) = g(r) \cdot \langle \Delta v_n^-(r) \rangle. \tag{8.4}$$

If the collision is so frequent particles are not able to respond to the flow between successive collisions and therefore the regime behaviour is dominated by inter-particle rather than hydrodynamic interaction (Ten-Cate *et al.* 2004). Consistent with this principal we observe in Lashgari *et al.* (2016) that the collision kernel is higher for the inertial shear-thickening regime than the one of the turbulent regime.

We therefore show that particle dynamics in the suspensions provide an additional evidence for the existence of two different mechanisms in the Bagnoldian regime that are driven by Reynolds stress and particle stress respectively.

CHAPTER 9

Conclusions & Outlook

9.1. Global stability analysis of complex flows

In the first part of the thesis we have studied the global instability behavior of non-Newtonian fluids in several classical configurations; cylinder flow, lid driven cavity flow and channel flow. We have employed both inelastic, Carreau, and elastic models, Oldroyd-B and FENE-P, to examine the shear-thinning, shear-thickening and viscoelastic features of the non-Newtonian fluids in the framework of linear stability analysis. Modal, nonmodal and sensitivity analysis have been employed to study the instability dynamics. The instabilities are interpreted by means of perturbation kinetic energy analysis.

The non-Newtonian effects significantly alter the characteristic of the underlying basic flows. For the flows around the cylinder and in a lid driven cavity, these alterations are observed in the size of the recirculating region, boundary layer thickness and vorticity intensity. In general, we have shown that the shear-thinning/shear-thickening effects destabilize/stabilize the cylinder and cavity flows. The frequency of the unstable modes increases/decreases with the shear-thinning/thickening effects. For the cylinder flow, the instability mechanism remains almost unchanged with the non-Newtonian effects, however the flow exhibits new instabilities in the shallow cavity of highly shear-thinning fluids and square cavity of highly shear-thickening fluids. Viscoelasticity affects the instability dynamics of the channel flow depending on the ratio between the viscoelastic and the flow time scales. For small/large values of this ratio the flow is destabilized/stabilized significantly. Transient growth of the streaks increases with elasticity while it first increases and then monotonically decreases for the oblique modes. In all the flow cases studied, the modifications of the instability dynamics are found to be strongly connected to the contribution of the different terms in the perturbation kinetic energy budget.

In this part, we have also examined the instabilities of Newtonian flow in X-junction by means of three-dimensional global stability analysis and direct numerical simulations. For all the velocity ratios between side and main channels, the flow exhibits two bifurcations by increasing the Reynolds number where the critical conditions are found to be independent of the inlet velocity of the main channel. Direct numerical simulations show that the first bifurcation is supercritical and the second one is weakly subcritical. We have sought a control strategy for the flow in X-junction based on the sensitivity analysis to

boundary velocity modification. We show that the critical Reynolds number of the first bifurcation can be increased by 80 % when we apply optimal suction at the wall with an amplitude of just 3 % of the inlet velocity.

9.2. Inertial suspensions of finite size rigid particles

In the second part of the thesis we study inertial suspensions of finite size rigid particles by Direct Numerical Simulations. We employ Immersed Boundary Method with direct forcing developed by Uhlmann (2005) and modified by Breugem (2012) to account for the presence of finite size particles. We focus on neutrally buoyant particle suspensions in a double-periodic channel configuration. A wide range of the bulk Reynolds number, $500 \leq Re \leq 5000$ and particle volume fraction $0 \leq \Phi \leq 0.3$ are studied fixing the ratio between the channel height to particle diameter to $2h/d = 10$. The presence of inertia modifies both the bulk and local behaviors of the suspensions by altering the relative motion and mutual interactions between the particles and fluid, especially at high volume fractions.

First we study the momentum balance of the two phase flow and identify three different inertial regimes based on the contribution of three different terms in the stress budget. Laminar regime at low Φ and low Re where the contribution of the viscous stress is the strongest in the total budget. Turbulent regime at high Re and moderate values of Φ where Reynolds stress shows the major contribution to transfer the momentum across the channel. And inertial shear-thickening regime where the contribution of the particle stress is dominant. Inertial shear-thickening regime is defined as a regime where we observe a significant increase in the effective viscosity (normalized wall shear stress) of the suspension and this is attributed to the particle stress and not Reynolds stress.

We connect our results with the experimental work by Bagnold (1954) where he introduces macro-viscous and grain-inertia regimes at low and high shear rate in the suspension of finite size particle between two cylindrical drums. The Bagnold number, defined as a ratio between inertial to viscous stress, determines the flow regime. Our results show that, at different concentrations, the effective viscosity of the suspensions at $Ba > 70$ versus Bagnold number collapses on a same curve indicating that both Reynolds stress and particle dominated regimes may share similar Bagnold number while their underlying physical mechanisms are different.

We further examine the particle dynamics in the inertial suspensions. The distribution of the particles across the channel for the laminar cases show a preferential wall normal position for the particles due to the inertial Segre-Silberberg effect. In contrast, turbulent cases are characterised by more homogenised particle distributions across the channel. A significant accommodation of the particles is observed in the inertial shear-thickening cases which is attributed to shear-induced migration from the region of high to low shear.

Particle dispersion shows high values at turbulent regime and low values at laminar regime. The corresponding values for the inertial shear-thickening cases lie between the two regime suggesting that the particle dynamics in this regime is a combination of the other two regimes. This is also confirmed by showing that the particle velocity fluctuations in the particle dominated regime is closer to the turbulent regime at the wall and almost overlap with the one of the laminar regime in the core of the channel. Analysing pair-particle statistics, radial distribution function, relative velocity and collision kernel, display the strongest contact interactions in the inertial shear-thickening regime. Particle dynamics in the suspensions provide additional evidences for the existence of the three different regimes introduced above.

In this part we also study the transition of the channel flow from laminar to turbulence of dilute regime of the particle suspension. i.e. $\Phi \approx 0.001$. We show that the initial arrangement of the particles in wall normal position is important in whether or not transition occurs at Reynolds numbers close to the threshold. Particles act as a source of disturbance whose amplitude depends on the particle size and background shear at the particle position. Particles do not influence the energy growth process in the flow however they contribute in secondary stability, breakdown of the coherent structures (streaks) and transition promotion. Once the flow become turbulent, they contribute to sustain the turbulence at a Reynolds number lower than the one of the unladen flow by inducing disturbances.

9.3. Outlook

In future we would like to expand our knowledge in the field of finite size particle suspensions. Since in many applications the particles in a flow have a wide range of sizes (poly-disperse), we would like to examine this effect by simulating the particle suspensions of two different sizes as the first step. In particular we plan to study the turbulent channel flow at a fixed Reynolds number and particle volume fraction, changing the ratio between the volume fraction of the small and large particles. To perform the simulations we will use a version of the IBM code developed and explained in Costa *et al.* (2015) where a new collision model is implemented including both normal and tangent collision force. Another important aspect in the suspension of finite size particles is the particle size effect. Particle size is kept constant throughout the present study, $2h/d = 10$. The smaller the particle size we consider in the simulation, the higher the computational cost needed for the simulations. We plan to examine the features of the suspension channel flow at both low and high Reynolds numbers, fixing the volume fraction, where the particle size are considered two and three time smaller than the one of the current study.

Summary of Papers

Paper 1

First instability of the flow of shear-thinning and shear-thickening fluids past a circular cylinder.

The flow past a cylinder is one of the most common configurations of the bluff body flows. It is well-known that the dynamics of the cylinder flow is intrinsic and it behaves like a global oscillator (Huerre & Monkewitz 1990). The first bifurcation of the Newtonian flow occurs at $Re \approx 47$ where a symmetric steady state becomes time-periodic with the appearnce of vortex shedding (Provansal *et al.* 1987).

In this paper, we have studied the onset of the first instability of the Carreau fluids flowing past a circular cylinder. We have employed the structural sensitivity analysis, the sensitivity analysis to base flow modification and energy analysis to examine the mechanism responsible for the onset of the instabilities.

We have shown that the first bifurcation occurs under the action of two-dimensional modes, as for the Newtonian flow. The critical Reynolds number of the pseudoplastic fluids decreases monotonically with the shear-thinning effects while the frequency of the unstable mode increases. The opposite trend is observed for the dilatant fluids. In all the cases considered, the core of instability consists of two lobes located symmetrically downstream of the cylinder. Shear-thinning/thickening effects shrink/diffuse the area of maximum sensitivity while increase/decrease the peak value of the sensitivity function. The results of sensitivity analysis to base flow modification remain almost unaffected by shear-thinning and shear-thickening effects and the maximum sensitivity is always localized close to the upper and lower sides of the cylinder surface. We have shown that the viscosity fluctuation does not play an important role on the neutral curve and stability mechanism of the flow. However, it contributes to amplify the perturbation kinetic energy downstream of the wave-maker region in the case of pseudoplastic fluids, while the opposite applies to dilatant fluids. Non-Newtonian effects modify the underlying base flow considerably. Reduction in drag coefficient, elongation of the recirculation bubble and intensification in the vorticity of shear layer are among the major modifications induced by shear-thinning. Interestingly for all pseudoplastic and dilatant cases

studied, we have found a critical length for the recirculation region above which flow start to bifurcate. Moreover, the spatial structure of the local Reynolds number (defined by the local viscosity) displays a value around 47 in the area of the largest structural sensitivity. Finally to tackle the issue of the choice of the reference viscosity in the definition of the Reynolds number, we have defined a reference viscosity by weighting the local viscosity with the norm of the structural sensitivity. We have shown that the critical Reynolds number based on the new reference viscosity is about 47 for all the cases.

Paper 2

Stability of fluids with shear-dependent viscosity in the lid-driven cavity.

Lid driven cavity flow is an another classical flow configuration with internal recirculating flows induced by the motion of one or more surrounding walls (see Shankar & Deshpande 2000). The Newtonian cavity flow, when the flow is assumed to be homogeneous in spanwise direction and the aspect ratio is equal to one (square cavity), first becomes unstable at $Re \approx 786$ due to the action of a stationary and three-dimensional global mode (Albensoeder *et al.* 2001).

In this paper we have examined the instability of a shear-dependent viscosity fluid in a lid-driven cavity with span-wise length of infinity. Two aspect ratios have been considered corresponding to square cavity, $\Gamma = 1$, and shallow cavity, $\Gamma = 0.25$. The Carreau model has been used to describe the rheological properties of the fluid. We have employed the structural sensitivity and perturbation kinetic energy analysis to investigate the mechanism behind the instability of the flow in the linear framework.

Generally, the flow is destabilized by shear-thinning and stabilized by shear-thickening effects. This behavior has been explained by thinning the boundary layer and reducing the intensity of shear inside the cavity for pseudoplastic fluids and opposite for the dilatant fluids. For both square and shallow cavities, the critical average Reynolds number (defined by the average viscosity in the domain) is almost independent of the rheological parameters in an intermediate range. The critical mode for the square cavity changes from stationary to oscillatory when power index $n > 1.2$ and its corresponding wavenumber decreases by the factor of 2. For shallow cavity however, we observe a significant decrease in the frequency and wavenumber of the instability mode when $n < 0.5$. For square cavity the sensitivity region is aligned with the streamlines in the case of pseudoplastic fluids which suggests an inviscid centrifugal mechanism. However for dilatant fluids, it localizes on the lower left corner when $n = 1.2$ and close to the right wall when $n = 1.4$. The core of instability for the shallow cavity is located on a side of the cavity in the direction of the lid velocity. For the strong shear-thinning effect the maximum moves to the region close to the lower wall. This effects is accompanied by an increase in the average Reynolds number for the same rheological parameter. Finally, we have observed that

the area of the maximum production of the perturbation kinetic energy and structural sensitivity always collapse in the cavity flow opposite to what we have shown in the cylinder flow.

Paper 3

Linear stability analysis of channel flow of viscoelastic Oldroyd-B and FENE-P fluids.

Normal mode analysis predicts the first instability of Newtonian Poseuille flow at Reynolds number about 5772 (Orszag 1971). However, Poseuille flow amplifies perturbations due to the non-normality of the eigenmodes at much lower Reynolds number (Trefethan *et al.* 1993; Schmid & Henningson 2001). The amplification of energy might be large enough to bring up nonlinear effects and trigger transition to turbulence.

In this paper, we have employed modal and non-modal analysis to investigate the stability of non-Newtonian Poiseuille flow in the inertial regime. Both Oldroyd-B and FENE-P models have been used to examine the behavior of the flow with polymer additive. Perturbation kinetic energy analysis helps to shed light on the physical mechanism of the instabilities.

We have obtained that the ratio between polymer relaxation time and instability time scale, $W\omega_r$, categorizes the effect of polymer on the instability of flow. In both modal and non-modal analysis, the flow is destabilized for small values of this ratio and stabilized for the large values. The maximum destabilization is obtained for the ratio of order one.

Modal analysis: For $W\omega_r < 1$, polymer molecules are assumed inelastic and they do not contribute to alter the total dissipation in the flow. However, they modify the phase-shift between streamwise and wall-normal perturbation velocity and promote the instabilities by increasing the production of perturbation kinetic energy. At larger $W\omega_r$, polymer molecules can be stretched by the shear flow and the elastic effects stabilize the flow by reducing the total production in the flow.

Non-modal analysis: We have shown that the growth of streaks increases monotonically with W while the growth of oblique modes displays an initial increase followed by a monotonic decrease. We have found a scaling for the growth of the oblique modes by which all the curves collapse when we replace W by W/T_{max}, where T_{max} is the time of the maximum growth. The increment in the transient growth of the streaks is attributed to an increase in the production of disturbance kinetic energy. Opposite explanation holds for the reduction in the transient growth of the oblique modes. Finally, we have also examined the effects of the viscosity ratio, β, and the maximum extensibility of the polymer molecules, L, on the stability of flow. By increasing the polymer concentration, modal instabilities are suppressed and the variation of the non-modal growth with respect to the Newtonian cases increases linearly.

Elastic effect is enhanced by increasing the maximum extensibility of the polymer molecules so that exponential instabilities are destabilized and non-modal growth is marginally reduced.

Paper 4

The planar X-junction flow: stability analysis and control.

X-junction flow is a geometrically complex flow that is established by three inlet and one outlet channels. X-junction is an underlying configuration for several natural phenomena and industrial applications such as river-junction (Best & Reid 1984), flow-mixers (Nguyen & Wu 2005) and flow focusers (Joanicot & Ajdari 2005). In the latter case, it is desirable to maintain the symmetric flow downstream while increasing the speed of the process (Kinahan *et al.* 2011).

In this paper, we have studied the instabilities and examined a control strategy of the Newtonian flow through a X-junction. We have employed three-dimensional direct numerical simulation, global stability, sensitivity and energy analysis to understand the nature of the flow bifurcations in the X-junction. The first bifurcation of the flow is then controlled by applying the optimal suction/blowing at the walls based on the knowledge obtained by the sensitivity to boundary velocity modification.

For all the examined velocity ratios, the ratio between the side and main channel centerline velocity V_r, the X-junction flow experiences two bifurcations as the Reynolds number is increased. The first destabilization occurs under the action of two dimensional stationary global modes where flow bifurcates from a steady symmetric state to a steady asymmetric state (Pitchfork bifurcation). At higher Reynolds number, flow bifurcates again by the action of stationary three-dimensional global modes around the asymmetric basic state. For $V_r = 3$, we have found the first bifurcation at $Re \approx 82.5$ and the second bifurcation at $Re \approx 115$. We have shown that the critical conditions for both bifurcations are almost independent of the inlet velocity of the main channel and scale with the inlet velocity of side channels. At the first bifurcation, the core of instability and the region of maximum perturbation energy production are localized symmetrically at the edges of the two recirculation bubbles where a shear layer instability is active. At the second bifurcation, the maximum sensitivity and disturbance energy production are located at the center and at the edge of the larger bubble and point toward a lift-up mechanism. The nature of the bifurcations are also examined by nonlinear simulations. Results show that the first bifurcation is supercritical while the second one is weakly subcritical. Three-dimensional simulations at $Re \geq 110$ exhibit a nonlinear cycle: a two-dimensional asymmetric flow, the growth of a spanwise modulation, a time-dependent chaotic flow, breakdown and return to a nearly two-dimensional asymmetric flow. We have explained the nonlinear cycle by marching the linearized N-S equation in time about an artificial base flow constructed by the steady asymmetric base flow

and an unstable three-dimensional stationary mode. When the amplitude of the stationary mode is large enough, we have observed an oscillatory unstable mode which is exponentially growing around the artificial base flow. Finally, we have applied the optimal suction/blowing at the wall of the symmetric flows around the first bifurcation. We have shown that the critical Reynolds number is pushed from $Re = 82.5$ to $Re > 150$, when the blowing amplitude is only 3% of the inflow velocity. Blowing affects the flow by reducing the back flow at the recirculating bubble and thus increasing the entrainment.

Paper 5

Laminar, turbulent, and inertial shear-thickening regimes in channel flow of neutrally buoyant particle suspensions

In this work we study the inertial suspension of finite size neutrally buoyant particles in a channel. We employ Direct Numerical Simulation together with an Immersed Boundary Method to simulate the finite-size particles in the flow. A wide range of bulk Reynolds numbers and particle volume fractions is considered, $500 \leq Re \leq 5000$ and $0 \leq \Phi \leq 0.3$, while the ratio between the channel height to the particle diameter is fixed. The simulations are initialised by a high amplitude localised disturbance on top of the laminar velocity profile and random arrangement of the particles.

First we observe that at low Φ the transition from laminar to turbulent flow is sharp and occurs at a critical threshold lower than the one of the unladen flow. As we increase Φ it becomes more and more difficult to distinguish between the laminar and turbulent regime. In particular for the highest particle volume fraction studied, $\Phi = 0.3$, no distinctive threshold for the transition is observed and the fluctuations in the flow exhibit a regime values much lower than the one of the turbulent unladen flow at all the Reynolds numbers.

Analysing the stress budget of the two phase flow, three different regimes are identified based on the balance between the three contributions in the total stress budget. Laminar regime at low Re and Φ where the contribution of viscous stress is strongest in the total budget. Turbulent regime at high Re and relatively low Φ where Reynolds stress is mainly responsible for the momentum transfer across the channel. And inertial shear-thickening regime at high Φ where the flow dynamic is governed by the contribution of the particle stress. Inertial shear-thickening regime is defined as a regime where a significant enhancement in the effective viscosity of the mixture (normalised wall shear stress) is observed and this not attributed to the Reynolds stress but to the particle stress.

We further examine our data in connection to the seminal work by Bagnold (1954). Bognold defines two different regimes, micro-viscous and grain-inertia, at low and high shear rate respectively in the suspension of neutrally buoyant particles between the two concentric cylinders. We show that the Reynolds

stress and particles stress dominated regimes may share similar Bagnold number while their underlying physical mechanisms are different. This behaviour is further illustrated in **paper 6** where we show that the profiles of effective viscosity versus Bagnold number for different particle volume fraction collapses at $Ba \geq 70$ for all the particle concentrations studied.

Paper 6

Channel flow of rigid sphere suspensions: particle dynamics in the inertial regime

In this paper we extend the work in **paper 5** by focusing on the particle dynamics in different regimes. Employing the same setup as **paper 5** we examine particle local concentration, rms velocities, dispersion and collisions.

We first study the particle distribution as a function of wall normal coordinate. For the viscosity dominated flows, $\Phi < 0.1$ and $Re < 1000$, we observe that the the wall and core region of the channel is almost empty form the presence of particles and they tend to accumulate at certain wall-normal equilibrium positions due to the Segre-Silberberg effect. The turbulent particle-laden flow, $\Phi < 0.1$ and $Re > 1500$, is instead characterised by a more uniform particle distribution due to turbulent mixing. For the particle dominated regimes, $\Phi > 0.2$, we report a significant migration of the particles toward the channel centreline for all the Reynolds numbers investigated. This not an inertial effect and occurs even at zero Reynolds number due to the shear-induced migration form the region of high to low shear rate.

The particle mean velocity profile changes from a parabolic type to more blunt when the flow regime changes from laminar to either turbulent or particle-dominated shear-thickening. The profile of the velocity fluctuations for the cases pertaining the inertial shear-thickening show similar values as those of the turbulent flow in the near wall region while they almost overlap to those of the laminar cases in the core region. This suggests that the particle dynamics in the inertial shear-thickening regime share similarities with both the laminar and turbulent regimes depending on the wall-normal position. Finally, we note that both the mean and fluctuating particle velocities exhibit slip velocities at the wall.

We also examine the particle dispersion in spanwise and wall-normal directions. Turbulent regime exhibits the highest and laminar regimes the lowest particle dispersion. The dispersion coefficients of the inertial shear-thickening regime lie in between those of the two other regimes. This is explained by the fact that in this regime turbulent activity is limited to the near-wall region while in the centre of the channel the particles form a dense layer and transported by the laminar like carrier flow.

Next we study the pair particle statistics, radial distribution function, $g(r)$, the approaching relative velocities, $\langle \Delta v_n^-(r) \rangle$, and the collision kernel, in different regimes. The laminar cases show the highest values of $\langle \Delta v_n^-(r) \rangle$ and

$\kappa(r)$ while the turbulent flows exhibit lower values due to the homogeneity created by the turbulent eddies. The accommodation of the particles in the core region of the cases pertaining inertial shear-thickening reduces $\langle \Delta v_n^-(r) \rangle$ and $\kappa(r)$ with respect to the turbulent cases.

In summary we show that the particle dynamics clearly reflects the existence of the three different flow regimes. The Bagnold number is shown to correctly predict the bulk flow behaviour for the parameter range of this study, however the details of the momentum transport and dissipation are different in the turbulent and particle-dominated regimes.

Paper 7

Transition and self-sustained turbulence in dilute suspensions of finite-size particles

In this work we study the transition to turbulence of dilute suspension ($\Phi \approx 0.001$) of finite size particles in a channel flow. The particle size is kept fixed, $2h/d = 10$, where h is half channel height and d is the particle diameter. We observe that the turbulence is sustained in the box to $Re_c \approx 1675$, a value lower than the one of the unladen flow $Re_c \approx 1775$; the large particles induces enough disturbances to sustain the turbulence at lower Reynolds number.

Simulating the flow at Reynolds numbers close to the threshold without any initial disturbance, the initial arrangement of the particles determines whether the flow experiences the transition or not. Each particle can be considered as a localised source for the disturbance. The amplitude and length scale of the disturbance depend on the background shear and the particle size. Since the particle size is kept fixed, the more the particles are positioned initially close to the wall, the transition is more likely to occur, because they induce more initial growth in the energy. On the other hand, if particles are not able to produce enough energy, the flow returns to its laminar state and the particles migrate towards their equilibrium position close to the centre of the channel.

Finally we compare the energy spectra of the cases where transition triggers with those that laminar state recovers. Results indicate that the transition is due to higher energy content in oblique disturbance modes. The particles induce strong enough oblique modes that promote the streak breakdown and transition to turbulence.

Acknowledgements

I would like to first acknowledge the support of my supervisor, Prof. Luca Brandt. I wish to thank him for giving me the opportunity to conduct my research in his group and for preparing a ground for me to get to know and work with many researchers around the world. Luca, *grazie mille!* Second, I thank my co-advisors, Prof. Dan Henningson and Dr. Fredrik Lundell for their guidance and discussions along with this project.

I am always grateful to work with Dr. Flavio Giannetti whose endless help and courage motivate me to work and *submit* more and more. Flavio, *grazie mille anche a te!*. I am pleased to work with Dr. Francesco Picano on the particle suspension. I appreciate his patience and generosity in sharing his knowledge. Francesco, *molte grazie!*. It was an honor for me to work with Prof. Hugh Blackburn and Prof. Murray Rudman during my stay in Australia. I appreciate all their support and guidance. It has been a great pleasure to work with Dr. Jan O. Pralits, Dr. Wim-Paul Breugem, Prof. Matthew Juniper and Dr. Tamer Zaki. I am indebted to them for their valuable comments and discussions on the present work. I owe my gratitude to Prof. Rama Govindarajan and Dr. Dhrubaditya Mitra for being always helpful and sharing their vast knowledge. It has been a pleasant experience for me to work with Dr. Outi Tammisola. I appreciate her guidance and significant contribution in our common project. Finally, this thesis would not have been possible without the cooperation of my friends, Simon Haque, Mengqi Zhang and Vincenzo Citro. Thanks a lot guys:).

This thesis has been reviewed by Dr. Christophe Duwig. I would like to thank him for his valuable comments. The Swedish abstract is written by Prof. Ardeshir Hanifi. Ardeshir, *merci!*.

I am happy to have worked in a nice atmosphere provided by my colleagues in the department of mechanical engineering. I wish to first thank my nice roommates Armin, Nima and Taras. I wish to thank other people in the department including the ones who were here before; Matbry!, Alexandra, Nicolo, Azad, Troppo Forte!, Jacopo, Ugis, Adam, Shervin, Philipp, Clio, Mehdi, Electra, Dhiya, Nicolas, Prabal, Arash, Sagar, Anthony, Hamid, Jean-Christophe, Ekaterina, Ricardo, Sohrab, Antonio, Ellinor, Renzo, Marco, Timea, Danial, Zeinab-m, Yuli, Antonios, Onofrio, Johan, Qiang, Sasan, David, Lailai, Reza, Enrico, Amin, Pierre, Arghya, Joy, Sardina, Luca Biancofiore, Zeinab, Werner,

Milos, Ruth, George, Miriam, Gerardo, Soolmaz, Bram, Yukinori, CJ, Carolina, Malin and Heide.

Computer time provided by SNIC (Swedish National Infrastructure for Computing) at the Center for Parallel Computers (PDC), KTH, is gratefully acknowledged.

Last but not least I owe my deepest gratitude to my parents and my girlfriend Azin for all their endless patient and support.

Bibliography

Abbas, M., Climent, E., & Simonin, O. 2009 Shear-induced self-diffusion of inertial particles in a viscous fluid. *Physical Review E* **79**, 036313.

Abbas, M., Magaud, P., Gao, Y. & Geoffroy, S. 2014 Migration of finite sized particles in a laminar square channel flow from low to high Reynolds numbers. *Phys. Fluids* **26**, 123301.

Abbott, J. R., Tetlow, N., Graham, A. L., Altobelli, S. A., E. Fukushima, L. A. M. & Stephens, T. S. 1991 Experimental observations of particle migration in concentrated suspensions: Couette flow. *Journal of Rheology* **35**, 773.

Albensoeder, S., Kuhlmann, H. C. & Rath, H. J. 2001 Three-dimensional centrifugal-flow instabilities in the lid-driven-cavity problem. *Physics of Fluids* **13** (121).

Bagchi, P. & Balachandar, S. 2003 Fully resolved simulations of particle-turbulence interaction. *Physics of Fluids* **15**, 3496.

Bagnold, R. 1954 Experiments on a gravity-free dispersion of large solid spheres in a Newtonian fluid under shear. *Proc. Royal Soc. London. Series A. Math. and Phys. Sci.* **225**, 49–63.

Balachandar, S. & Eaton, J. 2010 Turbulent dispersed multiphase flow. *Annu. Rev. Fluid Mech.* **42**, 111–33.

Barkley, D., Blackburn, H. M. & Sherwin, S. J. 2008 Direct optimal growth analysis for timesteppers. *Int. J. Numer. Meth. Fluids* **57**, 1435–1458.

Batchelor, G. & Green, J. 1972 The determination of the bulk stress in a suspension of spherical particles to order c^2. *J. Fluid Mech.* **56**, 401–427.

Batchelor, G. K. 1970 The stress system in a suspension of force-free particles. *J. Fluid Mech.* **41**, 545–570.

Bec, J., Biferale, L., Cencini, M., Lanotte, A., Musacchio, S. & Toschi, F. 2007 Heavy particle concentration in turbulence at dissipative and inertial scales. *Physical Review Letters* **98**, 084502.

Bellani, G., Byron, M. L., Collignon, A. G., Meyer, C. R. & Variano, E. A. 2012 Shape effects on turbulent modulation by large nearly neutrally buoyant particles. *J. Fluid Mech.* **712**, 41–60.

Best, J. L. & Reid, I. 1984 Separation zone at open-channel junctions. *Journal of Hydraulic Engineering* **110**, 1588–1594.

Bird, R. B. 1976 Useful non-Newtonian models. *Annu. Rev. Fluid Mech.* **8**, 13–34.

Bird, R. B., Armstrong, R. C. & Hassager, O. 1987 *Dynamics of Polymeric Liquids*, , vol. 1. Second edition, Wiley-Interscience.

Boyer, F., Guazzelli, E. & Pouliquen, O. 2011 Unifying suspension and granular rheology. *Phys. Rev. Lett.* **107**, 188301.

Brady, J. & Bossis, G. 1985 The rheology of concentrated suspensions of spheres in simple shear flow by numerical simulation. *J. Fluid Mech.* **155**, 105–129.

Brady, J. & Bossis, G. 1988 Stokesian dynamics. *Annu. Rev. Fluid Mech.* **20**, 111–157.

Brandt, L. 2014 The lift-up effect: The linear mechanism behind transition and turbulence in shear flows. *European Journal of Mechanics B/Fluids* **47**, 80–96.

Breedveld, V., Van Den Ende, D., Tripathi, A. & Acrivos, A. 1998 The measurement of the shear-induced particle and fluid tracer diffusivities in concentrated suspensions by a novel method. *J. Fluid Mech.* **375**, 297–318.

Brenner, H. 1961 The slow motion of a sphere through a viscous fluid towards a plane surface. *Chemical Engineering Science* **16**, 242–251.

Breugem, W.-P. 2010 A combined soft-sphere collision/immersed boundary method for resolved simulations of particulate flows. *Proceedings of the ASME 2010 3rd Joint US-European Fluids Engineering Summer Meeting and 8th International Conference on Nanochannels, Microchannels, and Minichannels, Montreal, Canada* **21**, 11.

Breugem, W. P. 2012 A second-order accurate immersed boundary method for fully resolved simulations of particle-laden flows. *Journal of Computational Physics* **231**, 4469–4498.

Brown, E. & Jaeger, H. 2012 The role of dilation and confining stresses in shear thickening of dense suspensions. *J. Rheol.* **56**, 875.

Brown, E. & Jaeger, H. 2014 Shear thickening in concentrated suspensions: phenomenology, mechanisms and relations to jamming. *Reports on Progress in Physics* **77** (4), 046602.

Burton, T. & Eaton, J. 2005 Fully resolved simulations of particle-turbulence interaction. *J. Fluid Mech.* **545**, 67–111.

Butler, J. 2014 Suspension dynamics: moving beyond steady. *J. Fluid Mech.* **752**, 14.

Campbell, C. S. 1990 Rapid granular flows. *Annu. Rev. Fluid Mech.* **22**, 57–92.

Caporaloni, M., Tampieri, F., Trombetti, F. & Vittori, O. 1975 Transfer of particles in nonisotropic air turbulence. *Journal of Atmospheric Sciences* **32**, 565–568.

Chikkadi, V., Sameen, A. & Govindarajan, R. 2005 Preventing transition to turbulence: A viscosity stratification does not always help. *Physical Review Letters* **95** (264504).

Chomaz, J. M. 2005 Global instabilities in spatially developing flows: non-normality and nonlinearity. *Annu. Rev. Fluid Mech.* **37**, 357–392.

Chun, B. & Ladd, A. J. C. 2006 Inertial migration of neutrally buoyant particles in a square duct: An investigation of multiple equilibrium positions. *Phys. Fluids* **18**, 031704.

Costa, P., Boersma, B. J., Westerweel, J. & Breugem, W.-P. 2015 Collision model for fully-resolved simulations of flows laden with finite-size particles. *Physical Review E* **92**, 053012.

Cunha, F. D. & Hinch, E. 1996 Shear-induced dispersion in a dilute suspension of rough spheres. *J. Fluid Mech.* **309**, 211–223.

Dbouk, T., Lemaire, E., Lobry, L. & Moukalled, F. 2013 Shear-induced particle migration: Predictions from experimental evaluation of the particle stress tensor. *J. Non-Newtonian Fluid Mech.* **198**, 78–95.

Deshpande, A. P., Krishnan, J. M. & Kumar, S. 2010 *Rheology of Complex Fluids*. Springer.

Doering, C. R., Eckhardt, B. & Schumacher, J. 2006 Failure of energy stability in Oldroyd-B fluids at arbitrarily low Reynolds numbers. *J. Non-Newtonian Fluid Mech.* **135**, 92–96.

Drazin, P. G. 2002 *Introduction to hydrodynamic stability*. United Kingdom: Cambridge university press.

Drew, D. 1983 Mathematical modelling of two-phase flow. *Ann. Rev. Fluid Mech.* **15**, 261–291.

Eaton, J. & Fessler, J. 1994 Preferential concentration of particles by turbulence. *Inter. J. Multiphase Flow* **20**, 169–209.

Eckstein, E. C., Bailey, D. G. & Shapiro, A. H. 1977 Self-diffusion of particles in shear flow of a suspension. *J . Fluid Mech* **79**, 191–208.

Eggels, J. G. M. & Somers, J. A. 1995 Numerical simulation of free convective flow using the lattice-Boltzmann scheme. *Int. J. Heat Fluid Flow* **16**, 357–364.

Einstein, A. 1906 Eine neue bestimmung der moleküldimensionen. *Ann. Phys.* **19**, 230–247.

Elghobashi, S. 1994 On predicting particle-laden turbulent flows. *Applied Scientific Research* **52**, 309–329.

Fall, A., Lemaître, A., Bertrand, F., Bonn, D. & Ovarlez, G. 2010 Shear thickening and migration in granular suspensions. *Phys. Rev. Lett.* **105**, 268303.

Farrell, B. F. & Ioannou, P. J. 1996 Generalized stability theory. Part I: Autonomous operators. *J. Atmos. Sci* **53**, 2025–2040.

Ferrante, A. & Elghobashi, S. 2003 On the physical mechanisms of two-way coupling in particle-laden isotropic turbulence. *Physics of Fluids* **15**, 315.

Giannetti, F. & Luchini, P. 2007 Structural sensitivity of the first instability of the cylinder wake. *J. Fluid Mech.* **581**, 167–197.

Giesekus, H. 1982 A simple consititutive equation for polymer fluids based on the concept of the deformation-dependent tensorial mobility. *J. Non-Newtonian Fluid Mech.* **11**, 69–109.

Gore, A. & Crowe, C. T. 1989 Effect of particle size on modulating turbulent intensity. *Int. J. Multiphase Flow* **15**, 279–285.

Govindarajan, R. & Sahu, K. C. 2014 Instabilities in viscosity-stratified flow. *Annu. Rev. Fluid Mech.* **46**, 331–353.

Groisman, A. & Steinberg, V. 2000 Elastic turbulence in a polymer solution flow. *Nature* **405**, 53–55.

Gualtieri, P., Picano, F. & Casciola, C. M. 2009 Anisotropic clustering of inertial particles in homogeneous shear flow. *J. Fluid Mech.* **629**, 25–39.

Gualtieri, P., Picano, F., Sardina, G. & Casciola, C. M. 2012 Statistics of particle pair relative velocity in the homogeneous shear flow. *Physica D* **241**, 245–250.

Guazzelli, É. & Morris, J. 2011 *A Physical Introduction to Suspension Dynamics*. Cambridge Univ Press.

Gunzburger, M. D. 2003 *Perspectives in Flow Control and Optimization*. Society for Industrial and Applied Mathematics.

Haddadi, H. & Morris, J. F. 2014 Microstructure and rheology of finite inertia neutrally buoyant suspensions. *J. Fluid Mech.* **749**, 431–459.

Hampton, R., Mammoli, A., Graham, A., Tetlow, N. & Altobelli, S. 1997 Migration of particles undergoing pressure-driven flow in a circular conduit. *Journal of Rheology* **41**, 621.

Haque, S., Lashgari, I., Giannetti, F. & Brandt, L. 2012 Stability of fluids with shear-dependent viscosity in the lid-driven cavity. *J. non-Newtonian Fluid Mech* **173-174**, 49–61.

Huerre, P. & Monkewitz, P. 1990 Local and global instabilities in spatially developing flows. *Annu. Rev. Fluid Mech.* **22**, 473–537.

Jeffrey, D. & Acrivos, A. 1976 The rheological properties of suspensions of rigid particles. *AIChE Journal* **22** (3).

Joanicot, M. & Ajdari, A. 2005 Droplet control for microfluidics. *Science* **309**, 887–888.

Kidanemariam, A. G., Chan-Braun, C., Doychev, T. & Uhlmann, M. 2013 Direct numerical simulation of horizontal open channel flow with finite-size, heavy particles at low solid volume fraction. *New Journal of Physics* **15**, 025031.

Kim, E., Elghobashi, S. & Sirignano, W. 1998 On the equation for spherical-particle motion: effect of Reynolds and acceleration numbers. *J. Fluid Mech.* **367**, 221–253.

Kinahan, M. . E., Filippidi, E., Köster, S., Hu, X., Evans, H. M., Pfohl, T., Kaplan, D. L. & J., W. 2011 Tunable silk: Using microfluidics to fabricate silk fibers with controllable properties. *Biomacromolecules* **12**, 1504–1511.

Klinkenberg, J., Sardina, G., Lange, H. C. D. & Brandt, L. 2013 Numerical study of laminar-turbulent transition in particle-laden channel flow. *Phys. Rev. E* **87**, 043011.

Koch, D. & Hill, R. 2001 Inertial effects in suspension and porous-media flows. *Annu. Rev. Fluid Mech.* **33**, 619–647.

Koh, C. J., Hookham, P. & Leal, L. 1994 An experimental investigation of concentrated suspension flows in a rectangular channel. *J. Fluid Mech.* **266**, 1–32.

Konijn, B., Sanderink, O. & Kruyt, N. 2014 Experimental study of the viscosity of suspensions: Effect of solid fraction, particle size and suspending liquid. *Powder Technology* **266**, 61–69.

Kulkarni, P. & Morris, J. 2008 Suspension properties at finite Reynolds number from simulated shear flow. *Phys. Fluids* **20**, 040602.

Lambert, R., Picano, F., Breugem, W. P. & Brandt, L. 2013 Active suspensions in thin films: nutrient uptake and swimmer motion. *J. Fluid Mech.* **733**, 528–557.

Lanzerstorfer, D. & Kuhlmann, H. C. 2012 Global stability of multiple solution in plane sudden-expansion flow. *J. Fluid Mech.* **702**, 378–402.

Larson, R. G. 1992 Instabilities in viscoelastic flows. *Rev in Rheological Acta* **31**, 213–263.

Lashgari, I., Picano, F., & Brandt, L. 2015 Transition and self-sustained turbulence in dilute suspensions of finite-size particles. *Theoretical and Applied Mechanics Letters* **5**, 121–125.

Lashgari, I., Picano, F., Breugem, W.-P. & Brandt, L. 2014 Laminar, turbulent and inertial shear-thickening regimes in channel flow of neutrally buoyant particle suspensions. *Phys. Rev. Lett.* **113**, 254502.

Lashgari, I., Picano, F., Breugem, W.-P. & Brandt, L. 2016 Channel flow of rigid sphere suspensions: particle dynamics in the inertial regime. *Inter. J. Multiphase Flow* **78**, 12–24.

Lashgari, I., Pralits, J. O., Giannetti, F. & Brandt, L. 2012 First instability of the flow of shear-thinning and shear-thickening fluids past a circular cylinder. *J. Fluid Mech* **701**, 201–227.

Leighton, D. & Acrivos, A. 1987 Measurement of shear-induced self-diffusion in concentrated suspensions of spheres. *J . Fluid Mech.* **177**, 109–131.

Li, Y., McLaughlin, J. B., Kontomaris, K. & Portela, L. 2001 Numerical simulation of particle-laden turbulent channel flow. *Physics of Fluids* **13**, 2957.

Loisel, V., Abbas, M., Masbernat, O. & Climent, E. 2013 The effect of neutrally buoyant finite-size particles on channel flows in the laminar-turbulent transition regime. *Phys. Fluids* **25**, 123304.

Lomholt, S. & Maxey, M. 2003 Force-coupling method for particulate two-phase flow: Stokes flow. *Journal of Computational Physics* **184**, 381–405.

Lu, J., Fernandez, A. & Tryggvason, G. 2005 The effect of bubbles on the wall drag in a turbulent channel flow. *Phys. Fluids* **17**, 095102.

Luchini, P. & Bottaro, A. 2014 Adjoint equations in stability analysis. *Annu. Rev. Fluid Mech.* **46**, 493–517.

Lumley, J. L. 1973 Drag reduction in turbulent flow by polymer additives. *J. Polymer Science* **7**, 263–290.

Maday, Y. & Patera, A. 1989 Spectral element methods for the incompressible Navier-Stokes equations. *In State of the Art Surveys in Computational Mechanics, ASME, New York* pp. 71–143.

Marchioro, M., Tanksley, M. & Prosperetti, A. 1999 Mixture pressure and stress in disperse two-phase flow. *Int. J. Multiphase Flow* **25**, 1395–1429.

Marchioro, M., Tanksley, M. & Prosperetti, A. 2000 Flow of spatially non-uniform suspensions. Part I: Phenomenology. *Int. J. Multiphase Flow* **26**, 783–831.

Marquet, O. & Sipp, D. 2010 Active, steady control of vortex shedding: An adjoint-based sensitivity approach. *Seventh IUTAM Symposium on Laminar-Turbulent Transition, IUTAM Bookseries* **18**, 259–264.

Marquet, O., Sipp, D. & Jacquin, L. 2008 Sensitivity analysis and passive control of cylinder flow. *J. Fluid Mech.* **615**, 221–252.

Matas, J. P., Morris, J. F. & Guazzelli, E. 2003 Transition to turbulence in particulate pipe flow. *Physical Review Letter* **90** (014501).

Matas, J. P., Morris, J. F. & Guazzelli, E. 2004 Lateral forces on a sphere. *Oil and Gas Science and Technology - Rev. IFP* **59** (59-70).

Maxey, M. & Riley, J. J. 1983 Equation of motion for a small rigid sphere in a nonuniform flow. *Physics of Fluids* **26**, 883.

Mittal, R. & Iaccarino, G. 2005 Immersed boundary method. *Annu. Rev. Fluid Mech* **37**, 239–261.

Mondy, L. A., Brenner, H., Altobelli, S. A., Abbott, J. R. & Graham, A. L. 1994 Shear-induced particle migration in suspensions of rods. *Journal of Rheology* **38**, 444.

Morrison, F. 2001 *Understanding Rheology*. Oxford university press.

Mullen, P. F. . J. 2001 Filter-based stabilization of spectral element methods. *Sciences - Series I - Mathematics* **332**, 265–270.

Nguyen, N. G. & Wu, Z. 2005 Micromixers - a review. *Journal of Micromechanics and Microengineering* **15**.

Nott, P., Guazzelli, E. & Pouliquen, O. 2011 The suspension balance model revisited. *Physics of Fluids* **23**, 043304.

Nott, P. R. & Brady, J. F. 1994 Pressure-driven flow of suspensions : Simulation and theory. *J. Fluid Mech.* **275**, 157–199.

Nouar, C., Bottaro, A. & Brancher, J. P. 2007 Delaying transition to turbulence in channel flow: revisiting the stability of shear-thinning fluids. *J. Fluid Mech.* **592**, 177–194.

Orszag, S. A. 1971 Accurate solution of the Orr-Sommerfeld stability equation. *J. Fluid. Mech* **50**, 689–703.

Patera, A. T. 1984 A spectral element method for fluid dynamics: Laminar flow in a channel expansion. *J. Computational Physics* **54**, 468–488.

Pearson, J. R. A. 1976 Instability in non-Newtonian flow. *Annu. Rev. Fluid Mech.* **8**, 163–181.

Peskin, C. 1977 Numerical analysis of blood flow in the heart. *Journal of Computational Physics* **25**, 220–252.

Phan-Thien, N. 2002 *Understanding viscoelasticity*. Springer.

Picano, F., Breugem, W.-P. & Brandt, L. 2015 Turbulent channel flow of dense suspensions of neutrally buoyant spheres. *J. Fluid Mech.* **764**, 463– 487.

Picano, F., Breugem, W.-P., Mitra, D. & Brandt, L. 2013 Shear thickening in non-Brownian suspensions: An excluded volume effect. *Phys. Rev. Lett.* **111**, 098302.

Pope, S. 2000 *Turbulent flows*. Cambridge University Press.

Pralits, J. O., Brandt, L. & Giannetti, F. 2010 Instability and sensitivity of the flow around a rotating circular cylinder. *J. Fluid Mech.* **650**, 513–536.

Procaccia, I., L'vov, V. S. & Benzi, R. 2008 Colloquium: Theory of drag reduction by polymers in wall-bounded turbulence. *Rev of Modern Physics* **80**, 225–247.

Prosperetti, A. 2004 The average stress in incompressible disperse flow. *Int. J. Multiphase Flow* **30**, 1011–1036.

Prosperetti, A. 2008 Ensemble averaging. *Applications of Science-Based Coupling of Models* **560**, 700.

Provansal, M., Mathis, C. & Boyer, L. 1987 Benard-von Karman instability: transient and forced regimes. *J. Fluid Mech.* **182**, 1–22.

Reade, W. C. & Collins, L. R. 2000 Effect of preferential concentration on turbulent collision rates. *Phys. Fluid.* **12**, 10.

Reek, M. W. 1983 The transport of discrete particles in inhomogeneous turbulence. *J. Aerosol Sci* **14**, 729–739.

Renardy, M. 1987 *Mathematical analysis of viscoelastic fluids*. Society for Industrial and Applied Mathematics.

Reynolds, O. 1883 An experimental investigation of the circumstances which determine whether the motion of water shall be direct or sinuous, and the flow of low resistance in parallel channel. *Phil. Trans. Roy. Soc. Lond. A* **174**, 935–982.

Saffman, P. G. 1965 The lift on a small sphere in a slow shear flow. *J. Fluid Mech.* **22**, 385–400.

Schmid, P. J. 2007 Nonmodal stability theory. *Annu. Rev. Fluid Mech.* **39**, 129–162.

Schmid, P. J. & Brandt, L. 2014 Analysis of fluid systems: stability, receptivity, sensitivity. *Applied Mechanics Reviews* **66**, 024803.

Schmid, P. J. & Henningson, D. S. 2001 *Stability and Transition in Shear Flows*. New York: Springer.

Segré, G. & Silberberg, A. 1961 Radial particle displacements in Poiseuille flow of suspensions. *Nature* **189**, 209–210.

Shankar, P. N. & Deshpande, M. D. 2000 Fluid mechanics in the driven cavity. *Annu. Rev. Fluid Mech.* **32**, 93–136.

Shaqfeh, S. G. 1996 Purely elastic instabilities in viscometric flows. *Annu. Rev. Fluid Mech.* **28**, 129–185.

Shewan, H. & Stokes, J. 2015 Analytically predicting the viscosity of hard sphere suspensions from the particle size distribution. *J. Non-Newt. Fluid Mech.* **222**, 72–81.

Sierakowski, A. & Prosperetti, A. 2015 Resolved-particle simulation by the Physalis method: Enhancements and new capabilities. *J. Computational Physics, in press* .

Soldati, A. & Marchioli, C. 2009 Physics and modelling of turbulent particle deposition and entrainment: Review of a systematic study. *Int J. Multiphase Flow* **35**, 827–839.

Squires, K. & Eaton, J. 1990 Particle response and turbulence modification in isotropic turbulence. *Physics of Fluids A* **2** (1191).

Squires, K. & Eaton, J. 1991 Preferential concentration of particles by turbulence. *Physics of Fluids A* **3** (1169).

Stickel, J. & Powell, R. 2005 Fluid mechanics and rheology of dense suspensions. *Annu. Rev. Fluid Mech.* **37**, 129–149.

Sundaram, S. & Collins, L. R. 1997 Collision statistics in an isotropic particle-laden turbulent suspension. Part 1. Direct numerical simulations. *J. Fluid Mech.* **335**, 75–109.

Tanner, R. I. 1985 *Engineering Rheology*. New York: Oxford university press.

Ten-Cate, A., Derksen, J., Portela, L. & Akker, A. V. D. 2004 Fully resolved simulations of colliding monodisperse spheres in forced isotropic turbulence. *J. Fluid Mech.* **519**, 233–271.

Theofilis, V. 2011 Global linear instability. *Annu. Rev. Fluid Mech.* **43**, 319–352.

Toms, B. A. 1949 Some observations of the flow of linear polymer solution through straight tubes at large Reynolds numbers. *Proceedings of the First International Congress on Rheology, Amsterdam* **2**, 135–141.

Trefethan, L. N., Trefethan, A. E., Reddy, S. C. & Driscoll, T. A. 1993 Hydrodynamic stability without eigenvalues. *Science* **261**, 578–84.

Tufo, H. M. & Fischer, P. F. 1999 Terascale spectral element algorithms and implementations. *Supercomputing, ACM/IEEE Conference* p. 68.

Uhlmann, M. 2005 An immersed boundary method with direct forcing for simulation of particulate flow. *J. Comput. Phys.* **209**, 448–476.

Uhlmann, M. 2008 Interface-resolved direct numerical simulation of vertical particulate channel flow in the turbulent regime. *Phys. Fluids* **20**, 053305.

Unverdi, S. O. & Tryggvason, G. 1992 A front-tracking method for viscous, incompressible, multi-fluid flows. *Journal of Computational Physics* **100**, 25–37.

White, C. M. & Mungal, M. G. 2008 Mechanics and prediction of turbulent drag reduction with polymer additives. *Annu. Rev. Fluid Mech.* **40**, 235–256.

Yeo, K. & Maxey, M. 2013 Dynamics and rheology of concentrated, finite-Reynolds-number suspensions in a homogeneous shear flow. *Phys. Fluid* **25**, 053303.

Yu, Z., Wu, T., Shao, X. & Lin, J. 2013 Numerical studies of the effects of large neutrally buoyant particles on the flow instability and transition to turbulence in pipe flow. *Phys. Fluids* **25**, 043305.

Zeng, L., Balachnadar, S., Fischer, P. & Najjar, F. 2009 Interactions of a stationary finite-sized particle with wall turbulence. *J. Fluid Mech.* **594**, 271–305.

Zhang, D. & Prosperetti, A. 1994 Averaged equations for inviscid disperse two-phase flow. *J. Fluid Mech.* **267**, 185–219.

Zhang, Q. & Prosperetti, A. 2010 Physics-based analysis of the hydrodynamic stress in a fluid-particle system. *Phys. Fluid* **22**, 033306.

Zhang, Z. & Prosperetti, A. 2003 A method for particle simulation. *J. Appl. Mech* **70**, 64–74.

Zhang, Z. & Prosperetti, A. 2005 A second-order method for three-dimensional particle simulation. *Journal of Computational Physics* **210**, 292–324.

Zhao, L. H., I., A. H. & Gillissen, J. J. J. 2010 Turbulence modulation and drag reduction by spherical particles. *Phys. Fluids* **22**, 081702.

Zhu, L., Lauga, E. & Brandt, L. 2012 Self-propulsion in viscoelastic fluids: pushers vs. pullers. *Phys. Fluids* **24**, 051902.